A single amino acid at PNT domain of ERG mediates its leukemogenic activity through interaction with the NCoR-HDAC3 co-repressor complex

Eitan Kugler
Tel Aviv University
Shreyas Madiwale
Tel Aviv University
Darren Yong
University of Toronto
Yehudit Birger
Schneider Children's Medical Center
Julie Thoms
Adult Cancer Program, Lowy Cancer Research Centre, UNSW Sydney, NSW 2052, Australia.
David Sykes
Harvard University, Cambridge,
Muhammad Yassin
Tel Aviv University
Nasma Aqaqe
Tel Aviv University
Avigail Rein
sheba medical center
Hila Fishman
Schneider Children's Medical Center
Ifat Geron
Tel Aviv University
Chun-Wei Chen
City of Hope https://orcid.org/0000-0002-8737-6830
Brian Raught
University of Toronto
Qiao Liu
City of Hope
Michael Milyavsky
Sackler Faculty of Medicine, Tel-Aviv University, Tel-Aviv, Israel

John Pimanda
Adult Cancer Program, Lowy Cancer Research Centre, UNSW Sydney, NSW 2052, Australia.
https://orcid.org/0000-0002-0509-8962
Gilbert Privé
University of Toronto https://orcid.org/0000-0002-0712-4319
Shai Izraeli (**sizraeli@gmail.com**)
Schneider Children's Medical Center https://orcid.org/0000-0002-6938-2540

Article

Keywords:

Posted Date: March 17th, 2022

DOI: https://doi.org/10.21203/rs.3.rs-1426447/v1

Version of Record: A version of this preprint was published at Nature Communications on September 21st, 2023. See the published version at https://doi.org/10.1038/s41467-023-41067-2.

Abstract

The ETS transcription factor ERG is involved in several cancers including leukemias. We and others have demonstrated a direct role for ERG in leukemia initiation and maintenance of several subtypes of myeloid and lymphoid leukemias. However, ERG domains and co-factors involved in leukemogenesis remains largely uncharacterized and as a transcription factor it is undruggable. Here we report a critical role for the conserved amino-acid proline at position 199, at the 3' end of the PNT domain, for ERG's leukemogenic activity. Specifically, we demonstrate that it is required for ERG-induced self-renewal and restriction of myeloid differentiation in hematopoietic progenitor cells and for initiation of leukemia in mouse transduction/transplantation models. Mechanistically, we show that P199 facilitates the interaction of ERG with the NCoR-HDAC3 co-repressor complex. Inhibition of HDAC3 reverses ERG's restriction of myeloid differentiation and reduces human ERG-dependent leukemic burden in immunodeficient mice. Thus, the interaction of ERG with the NCoR-HDAC3 co-repressor complex is required for its oncogenic activity and modulation of this interaction may provide an opportunity for therapeutic intervention.

Introduction

The human *ERG* gene belongs to the ETS family of transcription factors and is located on the long arm of chromosome 21 within the Down syndrome critical region [1–4]. In hematopoiesis, ERG supports self-renewal and functional properties of hematopoietic stem cells (HSC), as observed in mice carrying an *Erg* germline mutation in the ETS DNA binding domain [5, 6]. Similarly, *Erg* knockout in mice results in a rapid loss of self-renewing hematopoietic stem and progenitor cells (HSPC) due to premature differentiation [7]. Chromatin immunoprecipitation and sequencing (ChIP-Seq), integrated with gene expression analysis demonstrated that ERG is part of a "heptad" of transcription factors (TAL1, LYI1, LMO2, GATA2, RUNX1, ERG, FLI1), physically and functionally interacting with key cis-regulatory regions in HSC. Combinatorial interactions between these transcription factors direct HSPC function and fate [8–10].

When aberrantly expressed, ERG is a hematopoietic oncogene. High levels of ERG expression was associated with decreased overall survival in a study of 84 patients with normal karyotype acute myeloid leukemia (AML) [11]. In another cohort of 210 AML patients with normal karyotype, ERG expression was one of the strongest predictors of treatment outcome in a multivariable analysis [12]. We previously reported a mouse model transgenic for human ERG designed to clarify if ERG directly promote acute leukemia [13, 14]. By five months of age mice developed either T- ALL (30% of cases) or AML (70% of cases), characterized by a stem cell gene expression signature similar to human AML [13]. However, the molecular mechanisms that account for ERG oncogenesis in acute leukemia are mostly unknown.

Chromosomal translocations and structural aberrations related to ERG have been reported in AML, including the *FUS-ERG* and the *ELF4-ERG* fusion genes [15, 16]. Moreover, a RAG dependent *ERG* deletion or alternative transcript, following DUX4-IGH rearrangement, has been shown to promote B-cell precursor

acute lymphoblastic leukemia (ALL) with a favorable outcome [17, 18]. Co-expression of ERG and the short isoform of Gata1 (Gata1s, universally expressed in Down syndrome's myeloid malignancies), led to transient myeloproliferative disorder and acute megakaryocytic leukemia (AMKL) in mice [19–23]. Furthermore, ERG is associated with oncogenic protein complexes in human leukemia. For instance, the *CBFA2T3 (ETO2, MTG16)-GLIS2* fusion gene hijacks ERG to modify gene expression and the chromatin landscape of megakaryocytic precursors, resulting in differentiation arrest and AMKL development [24]. In another AML subtype associated with ETO proteins, ERG co-binds genomic regions with RUNX1-RUNX1T1 (ETO, MTG8, CBFA2T1) and its interacting partners, RUNX1, P300, and HDACs. The activity of ERG modulates RUNX1-RUNX1T1 expression, prevents oncogene overexpression, and maintains leukemia viability [25]. Finally, a recent study has demonstrated that ERG, in conjunction with members of the SWI-SNF complex and P300, mediates the leukemogenic process of the *TCF3-HLF* fusion gene in B lymphoid progenitors [26].

We demonstrated in a transgenic mouse that ERG is a leukemia oncogene [13, 20]. Here, we report that P199, a conserved proline at the C-terminal end of the ERG PNT domain, is essential for leukemic transformation. We further demonstrate that ERG interacts with the NCoR-HDAC3 complex, in a P199-dependent manner, to maintain HSPCs in an undifferentiated state. Consistent with this result, the chemical and genetic inhibition of HDAC3 in ERG-dependent human leukemia cells suppresses cell growth *in vitro* and ameliorates leukemia progression *in vivo*.

Results

Mutation of a single amino acid in ERG abrogates leukemia development.

To investigate the molecular mechanisms implicated in ERG-driven AML, we designed several transgenic mouse lines in which the expression of human ERG is regulated by the VAV promoter in HSPCs (TgERG). All mice developed AML or T-ALL by five months of age [13, 14, 20]. Fortuitously, during the construction of the first line of the ERG transgenic mice, a PCR error resulted in the substitution of an evolutionary conserved proline at position 199 by leucine (figure 1A and figure S1A and S1B). The mutant *ERG* RNA and protein were expressed in the spleen of transgenic mice (figure S1C). Immunoblot analysis of transfected CMK cells demonstrated that P199L ERG retains the nuclear localization of ERG (figure 1B). To study the effect of P199L on the structure and thermostability of the protein, we generated truncated and full-length versions of human ERG in *E. coli* (figure S2A*)*. High-performance liquid (HPLC) size-exclusion chromatography (SEC) was used to test whether P199L affects the hydrodynamic properties of ERG. Purified WT and P199L-ERG are monomeric in solution and monodisperse in SEC. The elution volumes of WT and P199L-ERG were indistinguishable, indicating that the mutation does not affect the hydrodynamic properties of the protein (figure 1C). Circular dichroism spectroscopy was used to assess differences in conformation and stability between ERG variants. The secondary structure and the thermostability of ERG were not significantly affected by P199L (figure 1D-E and S2B-C). Strikingly,

transgenic mice harboring the P199L variant were viable and did not show any signs of leukemia during their entire life span (figure S1D). Therefore, the P199 conserved amino acid plays a crucial role in ERG-mediated leukemogenesis. Regrettably, this first transgenic line of mice was discarded, thus no further analysis is possible.

P199L decreases the leukemic transformation of HSPC induced by ERG expression.

As P199L does not compromise the 3D structure, thermostability, or nuclear localization of ERG, we sought to evaluate its functional effects on HSPCs *in vitro* and *in vivo*. ERG dosage has been found to be critical to endow HSPC with aberrantly high self-renewal potential [19, 27, 7]. We therefore hypothesized, that the absence of leukemia in P199L-ERG transgenic mice was due to the decrease in self-renewal capacity of the transgenic HSPCs. To test this hypothesis, murine fetal liver-derived HSPC (C57BL/6 mice, E13.5, c-Kit^{+}/lineage negative cells) were transduced with a lentivirus expression vector of human ERG variants, followed by a re-plating assay in semi-solid conditions. HSPC transduced with P199L-ERG exhibited impaired self-renewal and colony-forming capacity as compared with the WT-ERG (figure 2A-B). The reduction in colony formation was not accompanied by a significant increase in apoptosis. (figure S3).

Next, we examined whether P199L-ERG expression influenced lineage commitment of HSPC. We used flow cytometry to measure the cell surface expression of murine HSPC markers c-Kit and Sca1, as well as megakaryocytic and myeloid cell markers, 72 hours after viral transduction with ERG variants (figure 2C-F). As we have previously shown [13, 22] ERG increased the percentage of c-Kit/Sca1 double positive HSPCs with megakaryocytic features, while blocking myeloid maturation. The P199L variant had the same effect as the WT-ERG on HSPCs and megakaryocytic markers but failed to block myeloid differentiation (figure 2E-F, expression of CD11b and Gr-1, $P<0.05$).

To independently confirm our initial observation in the transgenic mice regarding the leukemogenic potential of the WT and P199L-ERG isoforms, we carried out series of transduction-transplantation experiments. Murine fetal liver derived HSPCs transduced with human ERG variants were transplanted into sub-lethally irradiated C57BL/6 mice. During the 180-day observation period, all WT-ERG mice developed AML compared with 37.5% of P199L-ERG mice. Furthermore, the latency period for leukemia development was significantly longer in mutant mice (figure 3A-B) (Log-rank test, $P<0.0001$). The immunophenotype was comparable to what we previously reported for TgERG leukemia regardless of ERG variant, namely lineage negative, c-Kit^{low}, CD150^{+} AML. This population of cells is enriched with mega-erythroid progenitors (MEP, figure 3C) [13, 28].

Taken together, this suggests that ERG induced leukemic transformation is coupled with enhanced self-renewal capacity and restriction of HSPC myeloid differentiation; the P199L mutation disrupts these oncogenic functions.

P199L compromises the ERG transcriptional repression signature in HSPC.

To investigate how P199L affects ERG's transcriptional signature, RNA sequencing (RNA-seq) of murine fetal liver derived HSPCs expressing ERG variants was performed. Cells were cultured in serum-free media supplemented with SCF, TPO and FLT3, and collected for gene expression analysis 72 hours after transduction. Differentially expressed gene analysis indicated that P199L interferes with ERG-mediated transcriptional repression. As shown in figure 4A, gene sets that correlate with up-regulated genes are relatively evenly distributed among ERG variants. By contrast, transcriptional signatures associated with down-regulated genes are highly enriched for WT-ERG. These sets of genes include those found to be repressed in HSPC transformed by other leukemia-related oncogenes (HOXA9-MEIS1, NUP98-HOXA9). Interestingly, genes that were up-regulated upon NUP98-HOXA9 overexpression in HSPC ("NUP98-HOXA9 OE in HPC - up-regulated genes") were evenly enriched for both ERG variants. As previously demonstrated, *ERG* has been identified as a direct target of MEIS1, together with other stemness-associated genes, such as *CD34, FLT3* and *MYC* [29-32]. Our analysis reveals that the ectopic expression of ERG and MEIS1-HOXA9 oncogenes repress common set of target genes during AML development, which is compromised by the P199L mutation.

Moreover, specific genes normally up-regulated during myeloid differentiation were transcriptionally down-regulated in WT-ERG expressing cells compared with cells expressing P199L-ERG ("Myeloid differentiation - up-regulated genes", figure 4A-C), supporting the observed immunophenotype (figure 2E-F). Furthermore, CBFA2T3 transcriptional repression signatures in HSPC strongly correlated with WT-ERG (Figure 4A-C). The transcriptional co-repressor factor CBFA2T3 recruits the NCoR/SMRT complex together with class I HDACs to regulate HSC fate [33, 34]. In addition, it plays a crucial role in the development of pediatric AMKL in which CBFA2T3-GLIS2 interacts with ERG to promote leukemogenic activity [24]. Taken together, these results indicate that P199L substitution negatively affects ERG mediated repression of defined target genes, which are essential for AML development.

P199L disrupts the interaction of ERG with chromatin modifiers.

P199 is the last amino acid of the PNT domain, which structurally resembles the well-studied SAM protein interaction domain [35-37]. We hypothesized that P199L might, therefore, affect the interaction of ERG with one or more proteins essential to the progression of leukemia. We used proximity ligation-mass spectrometry (BioID) to compare proteins that localize in the proximity of WT vs P199L ERG in HEK293 cells [38]. A total of 240 putative protein interactors with a significance analysis of interactome (SAINT) [39] scores >0.8 and false discovery rate (FDR) <0.05 were identified. The hits were highly enriched with chromatin modifiers (figure S4), including 25 proteins associated with histone deacetylation. Notably, all the core components of the NCoR-HDAC3 complex were identified, including HDAC3, NCoR1, NCoR2, TBL1XR1, and GPS2, increasing the likelihood that the interaction is functionally meaningful (figure S4B). The second most prominent complex identified is the SWI/SNF (BAF) chromatin remodeling complex. We have identified 10 of the 14 core components of the BAF complex: SMARCB1, SMARCC1, SMARCC2, SMARCD1, SMARCD2, SMARCE1, ACTL6A, SMARCA4, ARID1A and ARID1B (figure S4B). In support of this result, it was recently shown by SILAC-based approach followed by mass spectrometry, that the TMPRSS2-ERG fusion oncoprotein interacts with canonical member of the SWI/SNF complex in a prostate cancer cell line [40].

To assess the effect of P199L mutation on the ERG BioID hits, we compared the proximity maps of WT-ERG and P199L-ERG (figure 5A-B and table S1). Globally, the P199L mutation resulted in a lower number of spectral counts in many of the hits, suggesting an impaired interactome. Remarkably, the largest effects were seen with the members of the NCoR-HDAC3 complex, with an approximate 40% reduction in the number of spectral counts for NCoR-HDAC3 complex members in comparison with WT-ERG (figure 5A-B).

To verify whether disruption of NCoR-HDAC3 complex interaction with ERG by P199L affects chromatin modifications of genes associated with leukemogenesis we stably expressed human WT and P199L ERG in the ER-Hoxb8 cell model of conditionally transformed hematopoietic progenitors that exhibit myeloid differentiation potential upon beta-estradiol withdrawal [41]. We used these isogenic cell lines to systematically investigate global effect of ectopic ERG and P199L-ERG expression on chromatin modifications by conducting chromatin immunoprecipitation (ChIP) sequencing coupled with transcriptome analysis.

We observed subtle differences in the global statistics of the ChIP signal enrichments (figure 6A). As we suspected an acetylation/deacetylation perturbation with P199L-ERG, due to the decreased interaction with NCoR-HDAC3 complex, we focused the analysis on the distribution of H3K27ac across the samples. We measured acetylation intensity at gene loci that exhibited differential expression and repression upon WT-ERG forced expression. We observed a decrease in H3K27ac signature at over 1500 unique sites in

cells transduced with WT-ERG compared to those transduced with the mutant (figure 6B-C). These gene loci were relatively hyperacetylated in both the control and P199L-ERG cells, compared to ER-Hoxb8 cells expressing WT-ERG (figure 6B-C). We observed less variation in the intensity of other types of histone modifications at those specific loci (figure 6B). These sites were predominantly associated with enhancers (co-occupancy of H3K27ac and H3K4me1) of genes expressed in mature myeloid cells (figure 6D-E). Intriguingly, variations in H3K27ac intensity between groups were less pronounced at transcription start sites (co-occupancy of H3K27ac, H3K4me3 and H3K9ac), (figure S5).

Collectively, these findings suggest that over expression of WT-ERG in myeloid progenitors reduces chromatin acetylation and activity at enhancer regions of genes expressed in mature myeloid cells. This in turn may restrict myeloid differentiation, as consistently demonstrated in AML.

HDAC3 inhibition alleviates the myeloid differentiation block induced by ERG expression in hematopoietic progenitors.

As demonstrated, the expression of ERG in HSPCs restricted myeloid differentiation (figure 2A) was accompanied by repression of myeloid differentiation genes via a decrease in the H3K27ac levels (figure 4 and 6). The proximity protein interaction map of ERG coupled with ChIP sequencing data suggested that this repression may be mediated by the recruitment of NCoR-HDAC3 repression complex to these ERG trans repression targets. To examine this hypothesis, we used the ER-Hoxb8 cells stably expressing human ERG as a model of myeloid differentiation. Upon removal of beta-estradiol from the growth medium, the ER-Hoxb8 cells differentiate into mature granulocytes over the course of five days [41] (Figure 7A).

As was demonstrated for murine fetal liver derived HSPCs (figure 2E and F), the proportion of Gr1-positive cells (marker for mature granulocytes) was significantly lower for ERG expressing ER-Hoxb8 cells in comparison to the cells transduced with backbone (BB) control vector (figure 7A). Consistent with the interaction of ERG with the NCoR-HDAC3 repressor complex, specific HDAC3 inhibitors (BRD3308 and RGFP966) [42, 43] alleviated the block in myeloid differentiation induced by ERG in ER-Hoxb8 cells (figure 7B). Moreover, the self-renewal capacity of murine fetal liver derived HSPC transduced with ERG was also compromised upon HDAC3 inhibition (figure S6).

Next, we addressed the role of HDAC3 in ERG's transcriptional activity. We treated human ERG expressing ER-Hoxb8 cells either with BRD3308 or DMSO for 48 hours and performed RNA sequencing. As shown in figure 7C, HDAC3 inhibition was associated with both de-repression and repression of target genes, but

the effect on de-repression was more pronounced. Interestingly, leukemia-associated pathways which were regulated by ERG in murine fetal liver derived HSPCs (Hoxa9-Meis1, CBFA2T3 and repression of myeloid differentiation genes) were ranked at the leading edge of gene sets that were significantly perturbed after HDAC3 inhibition (figure 7D). Particularly sensitive to HDAC3 inhibition were canonical pathways associated with differentiated myeloid cells (figure 7E-F).

HDAC3 inhibition attenuates ERG-dependent human AML cell growth in-vitro and in-vivo

To assay the significance of the ERG/NCoR-HDAC3 interaction in models of established leukemia, we treated human AML cells expressing high and low levels of ERG (figure S7A-C) [44] with an HDAC3 inhibitor (RGFP966) and examined its effect on cell proliferation. We reassessed ERG dependency of these leukemic lines by Cas9 mediated targeting of ERG. We found that genome editing of ERG resulted in the loss of leukemia cell growth accompanied by elevated apoptosis in the case of SKNO1 (AML harboring the RUNX1-RUNX1T1 translocation) and TF1 (erythroleukemia) cells, while THP1 cells were not affected by the ERG inactivation (figure 8A-B and figure S7B). In agreement with their ERG dependency, SKNO1 and TF1 cells were more sensitive to HDAC3 inhibition (figure 8C and figure S7C). To evaluate possible anti-leukemia effect of HDAC3 inhibition in vivo we utilized the SKNO1 leukemia model bearing a RUNX1-RUNX1T1 translocation that is addicted to ERG expression [25] (figure 8A-B) and dependent on HDAC3 activity (Figure 8C). NSG mice were treated intraperitoneally with 15 mg/kg RGFP966 for 21 days 24 hours following transplantation with 2.5 x 10^5 SKNO1 cells. RGFP966 exhibited a significant antileukemic effect as measured by the burden of disease in the bone marrow (figure 8D). This confirmed the importance of small molecule HDAC3 inhibition on the growth of SKNO1 cells *in vivo*.

As pharmacological inhibitors may induce off-target effects, we validated the importance of HDAC3 using genetic tools. It was previously shown that the KO of *Hdac3* in *Vav-Cre* transgenic mice led to dramatic defects in the growth of early hematopoietic precursors and failure to engraft in lethally irradiated mice [45]. We therefore aimed to decrease the expression of HDAC3 in SKNO1 cells (rather than a complete KO) due to concerns about cell death and poor engraftment following KO of HDAC3. The CRISPR-dCAS9 system was used in SKNO1 cells to decrease HDAC3 expression, followed by transplantation into NSG mice (figure S8A). Strikingly, leukemia development was abrogated in mice transplanted with SKNO1 cells with reduced expression of HDAC3 (follow up of 45 days) (figure 8E). This effect was translated into a significant survival advantage after a longer follow up period of 165 days (figure 8F). Interestingly, HDAC3 inhibition in THP1 cells had no effect on leukemia development *in vivo* (Figure 8G and figure S8B). Taken together, these results suggest that HDAC3 targeting in ERG-dependent AML has an anti-leukemic effect.

Discussion

ERG is a member of a core set of stem cell-specific genes expressed in both normal and leukemic stem cells and is linked to poor prognosis in AML. The molecular mechanisms by which ERG contributes to the development of AML are largely unknown. Here, we identified a single proline at the end of the PNT domain that is required for ERG leukemogenic function. Functional, genetic, and biochemical studies revealed that P199 contributes to the ERG-NCoR-HDAC3 interaction, thereby highlighting HDAC3 as a potential therapeutic target for ERG-mediated AML.

The failure to differentiate into mature myeloid cells is one of the hallmarks of AML.

We show that P199L negatively affects ERG-induced repression of myeloid differentiation genes and self-renewal of HSPC. Using a transgenic mouse model of AML, we have previously identified an ERG repressive gene expression signature [13](Fig. 1F in original paper). The ERG repressive gene expression signatures in HSPC strongly correlated with the signature of CBFA2T3 (ETO2, MTG16) and were impaired by P199L. CBFA2T3 is known to act in conjunction with the NCoR/SMRT/HDAC3 complex to regulate the expression of target genes in HSPC and MEP, thus controlling stemness and terminal differentiation[33, 34, 46–48]. CBFA2T3 and ERG have also been implicated in AMKL, where ERG expression was shown to be induced by the *CBFA2T3 - GLIS2* translocation and was critical for leukemic cell survival[24]. Our results show that P199L reduces the proximity based BioID signal to the NcoR-HDAC3 complex. Taken together, these findings support the hypothesis that, similar to CBFA2T3, ERG works in concert with NCoR-HDAC3 to restrict myeloid differentiation in HSPCs. In further support of this hypothesis, HDAC3 inhibition in human ERG-expressing murine HSPCs reversed the transcriptional and phenotypic effects of ERG by de-repressing genes normally expressed in mature myeloid cells.

ERG's role as a transcriptional repressor of cell differentiation was previously identified in prostate cancer, where aberrant expression of ERG inhibits the normal androgen receptor (AR) signaling pathway in coordination with transcriptional repression complexes [49]. ChIP-sequencing demonstrated co-binding of AR, ERG, HDAC1, HDAC2, HDAC3, and EZH2 on both promoters (HDAC1-dependent) and distal enhancer (HDAC3-dependent) to reprogram normal AR signaling and mediate transcriptional repression of cytoskeletal genes, which associate with epithelial differentiation. The de-repression of AR target genes upon treatment with a pan-HDAC inhibitor was much more significant in ERG positive prostate cancer cells than ERG negative prostate cancer cells [49, 50].

Chromatin dynamics control gene expression and lineage specification in hematopoiesis. The landscape of enhancers and super-enhancers define cell identity better than transcriptomic profile and promoter usage [51]. Cell fate specific enhancer establishment is initiated at the early stages of lineage commitment in progenitor cells and is marked by H3K4me1 (enhancer priming) [52]. The gain of H3K27ac is a late event during myeloid differentiation and is established together with active gene transcription once the cells are terminally differentiated. Together with MEIS1 and HOXA9, ERG was established as a regulator of hematopoietic stem cell enhancers [44, 53, 54]. Moreover, it was recently discovered that evolutionarily

conserved heptad enhancers in AML rely on ETS motifs for their activity [55]. Our findings suggest that ERG additionally restricts the activity of myeloid-specific enhancers in HSPC, as ERG forced expression led to a decrease in the H3K27ac signature at myeloid differentiation related gene loci associated mostly with H3K4me1. A gain in H3K27ac was detected for cells that were transduced with P199L-ERG at similar sites, thus supporting the hypothesis that the interaction with the NCoR-HDAC3 complex is essential for the process.

SKNO1 human AML cells carry the t(8;21) translocation fusing *RUNX1* with *RUNX1T1* that account for 7% of adult AMLs [56]. While RUNX1 is a transcription activator, RUNX1T1 was shown to act as a co-repressor by recruiting the NCoR-HDAC complex to regulatory elements of target genes [57, 58]. By replacing the transactivating domain of RUNX1 with almost the entirety of RUNX1T1, the oncogene generated by t(8;21) is thought to convert the RUNX1 transcriptional activator to a strong repressor [25, 59–61]. Analysis of the transcriptome and epigenome of t(8;21) patient cells revealed binding of ERG, FLI1, TAL1 and RUNX1 at all RUNX1-RUNX1T1 occupied regulatory regions. Knockdown of ERG resulted in cell death and was accompanied, surprisingly, by an increased expression of RUNX1-RUNX1T1, oncogenic overdose and cell lethality. ChIP-qPCR after knockdown of ERG revealed an increase in P300 and a decrease in HDAC1 occupancy at the promoter region of RUNX1-RUNX1T1[25]. Furthermore, a recent study has demonstrated that RUNX1 is a component of the NCoR-HDAC3 complex in t(8;21) AML and collaboratively represses RUNX1-RUNX1T1-dependent transcription, thereby linking HDAC3 directly to leukemogenesis associated with t(8;21)[62]. Taken together, the enhanced apoptosis observed in SKNO1 cells following HDAC3 inhibition could be explained by a co-regulatory function of ERG and the NCoR-HDAC3 complex in t(8;21) leukemic cells.

The development of HDAC inhibitors for therapy of hematopoietic malignancies originated from the observation that several compounds that were known to induce the differentiation of leukemic cell lines were HDAC inhibitors [63, 64]. However, the results of several clinical studies were disappointing [65, 66]. A pan-HDAC inhibitor was used in these clinical studies, and thus the role of specific types of HDACs in AML is not known. HDAC3-specific inhibition was recently tested in a mouse model of AML and was shown to be a useful target in combination with cytarabine. The synergistic effect of HDAC3 inhibition and cytarabine was mechanistically attributed to the involvement of the former in the DNA damage response [43].

Our findings indicate that the aberrant overexpression of ERG maintains HSPCs in an undifferentiated state and promotes AML development. We suggest that the interaction between ERG and the NCoR-HDAC3 complex has an important role in the leukemogenic process, and that HDAC3 inhibition could be beneficial in AML characterized by high ERG expression. ERG is a transcription factor and generally not considered as a druggable target. As such, the mechanism proposed here identifies HDAC3 inhibition as a potential therapeutic route for the treatment of ERG-driven and ERG-dependent leukemias. The recent identification of a similar mechanism of ERG mediated prostate cancer, suggests that this approach may have a general role in ERG driven malignancies.

Declarations

Acknowledgments

The authors thank Jonatan Barel, Gilgi Friedlander, Dayana Yahalomi and Avital Sarusi Portuguez from the Nancy and Stephen Grand Israel National Center for Personalized Medicine, Weizmann institute of science, for RNA-seq and ChIP-seq analysis service. The authors thank Brice Mouttet and the Bourquin lab for assistance in finalizing Co-IP protocols. We thank Ercument Dirice for sharing substantial information regarding BRD3308 handling in mice. The authors would also like to thank Rani Elkon for providing general bioinformatics guidance. We are indebted to Itzhak Ben Moshe (Ofer) for help in mice processing and in-vivo experiments. We thank all past and present members of S.I. research group for fruitful discussions and advice. This study was supported by the Israel Science Foundation, Dotan Research Center in Hemato-Oncology, the Waxman Cancer Research Foundation, CRISPR-IL consortium.

Autor contribution

Conceptualization and methodology, S.I, E.K, Y.B and S.M; Formal analysis, E.K, S.M and DY; Investigation, E.K, S.M, D.Y, J.I.T, B.R, A.R, Y.B, H.F and I.G; Resources, DBS, M.Y, N.A, C.C.W, A.R and M.M; Writing – original draft, E.K, S.I; Supervision, S.I, J.P, G.G.P and M.M.

Methods

Cells lines and primary cultures:

All the cells used were maintained at 37°C in 5% CO2. HEK 293T cells are human embryonic kidney cell line used routinely for virus preparations. The cells were grown in DMEM (Gibco) supplemented with 10% FBS (Gibco), 1% L-Glutamine, and 1% penicillin/streptomycin. Estrogen-regulated ER-Hoxb8 granulocyte-monocyte murine progenitors (GMP) were kindly provided by Prof. David Sykes at the Massachusetts General Hospital. It is a murine GMP cell line that conditionally expresses the ER-Hoxb8 oncoprotein under the regulation of the estrogen receptor. As estrogen is withdrawn from the culture media, the cells differentiate to mature neutrophils in a process that typically lasts five days [41]. Cells are grown in RPMI (Gibco) supplemented with 10% FBS (Gibco), 1% L-Glutamine, and 1% penicillin/streptomycin. In addition, 2% SCF and beta-estradiol (Sigma, E-2758) in a concentration of 0.5 micromolar are added to culture media. Primary murine fetal liver derived HSPC were cultured at 37°C in 5% CO_2 in serum free medium supplemented with (Stem Cell Technologies, StemSpan SFEM, #09605), % L-Glutamine, 1% penicillin/streptomycin, mSCF (10ng/ml, PeproTech), mTPO (10ng/ml, PeproTech) and mFLT3 (10ng/ml, PeproTech).

Animals

Pregnant C57Bl/6 female mice for transduction-transplantation assays were purchased from Envigo laboratory. For transplantation assays, six weeks old female C57Bl/6 mice were included in the study. Mice were housed in barrier facility. Animal studies were approved by Tel-Aviv University and Chaim Sheba Medical Center at Tel Hashomer Institutional Animal Care and Use Committees. The Helsinki ethics committee at the Chaim Sheba Medical Center authorized all in-vivo experiments (authorization number: 14-051M) for up to 800 mice during the years 2014-2018.

Vectors and mutagenesis:

Human cDNA of *ERG* was cloned to MA-1 bidirectional second-generation lentivirus expression vector [67]. The expression of *ERG* is regulated under the hPGK promoter, and the expression of GFP is regulated under the minimal CMV promoter. cDNA of human *ERG* was cloned to MA-1using Xba1 (5') and Sma1(3') restriction sites. The insert contained a Kozak sequence and an HA tag (5'). Site-directed mutagenesis was carried out to introduce the P199L mutation. Site-directed mutagenesis was carried out using the QuikChange II Site-Directed Mutagenesis Kit (catalog #200523) according to the manufacturer's instructions.

Enrichment of mouse hematopoietic stem and progenitors:

Pregnant mice (purchased from Envigo laboratory) were scarified on E13.5 and fetal liver cells were isolated. HSPC were enriched using the lineage positive depletion magnetic kit (Miltenyi Biotec MACS Lineage cell depletion kit,130-090-858). Lineage depleted cells were cultured at 37°C in 5% CO_2 in serum free medium supplemented with (Stem Cell Technologies, StemSpan SFEM, #09605), % L-Glutamine, 1% penicillin/streptomycin, mSCF (10ng/ml, PeproTech), mTPO (10ng/ml, PeproTech) and mFLT3 (10ng/ml, PeproTech).

Lentiviral experiments:

Lentiviral supernatants were generated by co-transfection of 293T cells with MA-1 as the expression vector and viral packaging plasmids psPAX2 and pMD2.G (Addgene ID 12260 and 12259 respectively). Cells were transfected using the calcium phosphate Profection Mammalian Transfection kit (Promega) according to the manufacturer's instructions. The supernatant was collected twice: at 24 and 48hr following transfection and filtered through a 0.45 μm strainer. The supernatant was concentrated using Vivaspin (Sartorius) for the transduction of ER-Hoxb8 cells. For the transduction of fetal liver derived HSPC, the supernatant was concentrated using ultracentrifuge (3:30hr, 20,000 rpm, 10◦C).

To transduce murine fetal liver derived HSPC, we cultured the primary cells in 96 well plates with serum-free medium conditions as described. Each well was cultured with 50,000 cells. The viral titer was aimed to be approximately 50 MOI. Five ug/ml Polybrene was added to each well. We used spinfection for transduction at a rate of 1000g for 90 minutes at 22°C. After centrifugation, the cells were incubated at 37°C in 5% CO2. Frothy-eight hours post-transduction, the cells were collected, washed, and used for further applications. The transduction efficiency was measured using flow cytometry for GFP.

Methylcellulose re-plating assays:

Murine fetal liver derived HSPC were transduced with MA-1 Lentiviruses expressing either WT-ERG, P199L-ERG, or an empty vector as a control. Ten thousand cells per construct were plated in duplicates of one ml methylcellulose supplemented with mIL-3, mIL-6, mSCF (Stem Cell Technologies mouse MethoCult M3534). Cells were incubated at 37°C in 5% CO2 for seven to ten days. Following incubation, colonies consisting of more than 50 cells were counted, and 10,000 cells were re-plated in duplicates in new methylcellulose cultures. GFP verified the presence of transduced cells.

Transduction-transplantation assays:

Murine fetal liver derived HSPC were enriched and transduced with expression vectors carrying ERG variants as described above. The transduction efficiency of each construct was evaluated by GFP percentage using Galios Flow Cytometer (Beckman-Coulter).

Six-week-old C57Bl/6 mice female recipient (purchased from Envigo) were administered a sublethal dose of 650 rad X-Ray irradiation 24hr prior to transplantation. Recipient mice received prophylactic antibiotic treatment 48 hours before transplantation and until 48 hours post-transplantation. 10^5 transduced cells together with $2x10^5$ BM support cells (freshly harvested from the bone marrow of C57Bl/6 mice and lysed for red blood cells) were resuspended in PBS and injected via the tail vein of irradiated recipients.

ER-Hoxb8 differentiation assay:

Stable cell lines of ER-Hoxb8 cells overexpressing *ERG* variants were created.

For viral transduction, 200,000 cells were cultured in 6 well plates in RPMI supplemented with 10% FBS (Gibco), 1% L-Glutamine, and 1% penicillin/streptomycin, 2% SCF and 0.5UM beta-estradiol as described above. Cells were transduced with a lentiviral containing expressing vectors of WT-*ERG*, P199L-*ERG*, and an empty vector. Lentiviral supernatant was added to each plate together with five µg/ml Polybrene. Cells were centrifuged for 1000g for 90 minutes at 22°C and were incubated at 37°C in 5% CO2. Frothy-eight

hours following spinfection, the transduction rate was measured using GFP and was generally 20-30%. GFP positive cells were then sorted and incubated at 37°C in 5% CO2 for one week. As cells recovered from the sorting procedure and proliferated, 50,000 ER-Hoxb8 cells were carefully washed to remove beta-estradiol remaining and re-cultured in 24 well plates in the ER-Hoxb8 medium as described above without beta-estradiol. We next assessed the differentiation rate of the cells towards mature granulocytes as a function cell construct. Flow cytometry was carried out using an antibody for Gr1 (APC, Biolegend). Mean fluorescence intensity was measured for comparison.

Flow cytometry:

Flow cytometry was used in determination transfection/ transduction efficiency, for cell count, and for immunophenotyping. For all the above, cells were washed in staining media (2%FBS in PBS) and re-suspended in 100µl staining media containing fluorochrome-conjugated antibodies for 30 min. Following staining, cells were washed with staining media, re-suspended to a final volume of 100µl staining media, and analyzed on a Gallios flow cytometer (Beckman-Coulter). All cell mixtures were stained with an appropriate color of Fixable Viability Dye (Life Technologies) to exclude dead cells from analysis. Quadrant gates were defined according to single stains and full minus one staining (FMO) of each fluorophore. Data were analyzed with FlowJo software (BD).

Western blot analysis:

$2X10^6$ cells were lysed using either RIPA buffer or CellLytic M (Sigma) with HALT protease inhibitor cocktail (Thermofisher). Protein lysates were separated on SDS gel and transferred to a nitrocellulose membrane. Membranes were blocked for 1hr with PBS-T containing 5% skim milk and were incubated at 4°C overnight with a primary antibody. Membranes were washed with PBS-Tween (0.05%) and incubated with a secondary antibody (1:10000, Jackson ImmunoResearch Laboratories) for 2hr at room temperature. The membrane was rewashed with PBS-T. Proteins were detected using enhanced chemiluminescence (ClarityTM Western ECL Blotting Substrates Bio-rad), and signals were detected using a gel documentation system (Bio-rad). For ERG expression and cellular sub-localization: 293T cells were transiently transfected with *ERG* expression vectors using the calcium phosphate Profection Mammalian Transfection kit (Promega). 48hrs following transfection, cells were collected, and cytoplasmatic or nuclear proteins were extracted using NucBuster Protein Extraction Kit (Novagen) according to the manufacturer's instructions.

For ERG immunoblot we used anti human ERG antibody by Santa Cruz (C-17, sc-354, 1:1000). For HA immunoblot we used anti-HA monoclonal antibody (Sigma, H3663). For Vinculin immunoblot we used anti Vinculin antibody manufactured by Abcam.

RNA sequencing:

Murine fetal liver derived HSPC were transduced with ERG variants as described above. All samples were sorted for GFP positive cells ($5x10^5$ cells/sample) by BD FACSAria, centrifuged (10min, 1200rpm), fluidized in TRIzol reagent, and purified using the TRIzolTM Plus RNA Purification Kit (Invitrogen). Sequencing and analysis were performed in the INCPM of Weizmann Institute of Science (The Crown Genomics institute of the Nancy and Stephen Grand Israel National Center for Personalized Medicine, Weizmann Institute of Science, Israel). RNA was purified, analyzed by bioanalyzer (Agilent 2100), and cDNA libraries were prepared using INCPM mRNA-seq. Genome-wide expression profiles were obtained by sequencing of the samples on Illumina HiSeq 2500 machine, SR60_V4. The output was approximately 24 million reads per sample. Resulting reads shorter than 30bp were discarded. Reads were mapped to the M. musculus reference genome GRCm38 using STAR. Differentially expressed genes were identified using DESeq2 in R software [68]. Raw P values were adjusted for multiple testing using the procedure of Benjamini and Hochberg.

GSEA

Gene set enrichment analysis was performed using a pre-ranked list [69]. All transcripts per sample with more than 30 reads were included in the analysis. The score for each gene was calculated as $\log_{10}$(p-value). Genes that were downregulated had a negative score and upregulated genes received a positive score. The Gene expression profile was compared to the MSigDB database (Broad). Adjusted q value of less than 0.05 was used as a cutoff for significance. Analysis was conducted using the R package ClusterProfiler [70].

Functional enrichment analysis

Over-representative analysis using g: Profiler was conducted for differentially expressed genes (adjusted p-value <0.05) in ER-Hoxb8 cells overexpressing ERG variants. The gene expression signature was compared between cells treated with an HDAC3 inhibitor to DMSO treated cells. A significance threshold of the adjusted p-value of 0.05 was used according to the g: SCS algorithm [71].

ChIP sequencing

ChIP material was prepared from ER-Hoxb8 cells stably expressing ERG variants and an empty vector for control. 10^7 cells were used per sample. Samples preparation and immunoprecipitation were conducted by the assistance of our collaborator Dr. Julie Thomas (Prof. John Pimanda's lab in Australia) and as previously described [13].

Briefly, cells were crosslinked with 1% paraformaldehyde for 15 minutes and were quenched with glycine for 5 minutes at room temperature. Lysis buffer with protease inhibitor was gently added to cell pellet. Fixed chromatin was sonicated with the Bioruptor Pico using pre-optimised conditions and immunoprecipitated with the indicated antibody. Immunoprecipitation was preform using polyclonal antibody raised against H3K27ac, H3K4me1, H3K4me3, H3K9ac (Abcam). As a control, nonspecific rabbit IgG (I5006; Sigma Aldrich) was used.

For sequencing and analysis: ChIP samples were amplified and sequenced using the Illumina HiSeq2500 machine, SR60_V4 (BGI). Median sequencing depth was ~25 million reads per sample. Adapters were trimmed using the Cutadapt tool. Following adapter removal, reads that were shorter than 30 nucleotides were discarded. Reads alignment and peak calling was performed at the INCPM of Weizmann Institute of Science (The Crown Genomics institute of the Nancy and Stephen Grand Israel National Center for Personalized Medicine, Weizmann Institute of Science, Israel). The reads were aligned uniquely to the mouse genome (mm10) using bowtie (version 1.0.0). Bound regions were detected using MACS2 (version 2.0.10.20131216). GREAT was used for assigning genomic regions to genes. HOMER (version 4.7) was used for obtaining statistics on ChIP enrichment of genome features.

Heatmaps and metagene plots of the genes with changed H3K27ac read coverage were plotted using the R package "Genomation" [72]. g: Profiler was used for functional enrichment analysis [71].

BioID and mutated ERG stability assays

Cloning of ERG plasmids:

All ERG constructs were subcloned from a mammalian expression MA-vector (described above) encoding for a N-terminal HA tag wild type and P199L ERG. The MA-vector was used as a template for PCR to generate ERG inserts. ERG PCR inserts were cloned by restriction enzyme digestion followed by T4 ligation into the corresponding destination vector. For bacterial expression, ERG 1-265 WT or P199L were cloned into the custom vector PSJ5. PSJ5 encodes for a fusion protein with a N-terminal TrxA – 6xHis – thrombin cleavage site – STag – enterokinase site – 8xHis – TEV cleavage site. For BioID, ERG 1-479 WT/P199L or eGFP were cloned into a piggybac vector encoding for a FLAG-BirA* N -terminal fusion protein.

Protein expression

PSJ5 expression plasmids were transformed into *E. coli* BL21-CodonPlus cells and selected on LB agar plates containing 100 µg/mL ampicillin. Starter cultures were grown overnight at 37 °C. Expression cultures were inoculated with a 1:40 volume ratio of starter culture in 0.5x TB medium supplemented with 100 µg/mL of ampicillin or 50 µg/mL of kanamycin. Cells were grown at 37 °C to an OD_{600} of 0.8-1.0 before inducing protein expression with 0.5 mM IPTG for 16-18 hr at 15 °C. Pellets were resuspended in Lysis Buffer (500 mM NaCl, 25 mM Tris pH 8, 1 mM βME with 400 µg of DNaseI (Sigma) and 1 cOmplete™ Protease Inhibitor Cocktail tablet) by vortexing. Cells were lysed by passage through an Emulsiflex for 15 minutes. The lysed cells were then centrifuged at 17,000 rpm for one hour at 4 °C to remove insoluble material. The supernatant was then filtered using a 0.45 µM syringe filter before purification.

Purification

His-tagged proteins were purified from the supernatant by gravity-flow Ni-NTA affinity chromatography (Qiagen). Where indicated, affinity tags were cleaved from the fusion proteins by TEV protease treatment at a 1:30 molar ratio of protease to protein, while dialyzing in the lysis buffer for 16 hours at 4 °C. Affinity tags were removed by Ni-NTA affinity chromatography and the proteins of interest were collected in the flow-through. Proteins were then concentrated and further purified by either S75 or S200 size exclusion column chromatography in the indicated assay buffer. Peak A_{280} fractions were concentrated, flash frozen and stored at -80 °C.

Circular dichroism spectrum scan and temperature melt

Proteins were dialyzed into CD Buffer (100 mM NaCl, and 25 mM $NaPO_4$ pH 7.5). Circular Dichroism (CD) experiments were performed on the Jasco J-810 Spectropolarimeter. Protein samples were diluted to 0.3 mg/mL and loaded into a 0.1 cm path length curvette. Spectrum scans were collected between 195-250 nm with a response of 8 sec/nm and averaging 5 readings per wavelength. Temperature range for thermal melts ranged from 20 to 95 °C collecting at 226 nm. Data was processed using Excel. Buffer only was used as a background control. Secondary structure content was estimated using a CD-spectra simulator and fitted to the experimental spectra in Excel (Abriata 2011).

Analytical size exclusion chromatography

Analytical size exclusion chromatography (SEC) was performed on a Waters Breeze 2 HPLC with a Shodex KW-803 size exclusion column. Samples were loaded in 110 µL volumes running at 0.8 mL/min in 150 mM NaCl, 25 mM Tris pH 8, 0.5 mM TCEP. Elution profiles were measured at 230 and 280 nm.

Stable cell line generation for BioID

Stable cell lines for BioID were generated in HEK293 GnT –/– cells. Cells were transfected using Lipofectamine 2000 according to the manufacturer protocol with a few changes. A total of 1 µg of DNA was used for transfection. The DNA mixture consisted of FLAG-BirA*-ERG 1-479 WT/P199L or eGFP control: PBase: PB-RB at an 8:1:1 molar ratio respectively. Transfected cells were selected by drug resistance to puromycin at 1 µg/mL and blasticidin at 0.5 µg/mL for 3 weeks.

Bait expression and biotin labelling

Drug resistant cells expressing inducible FLAG-BirA*-ERG 1-479 WT/P199L or eGFP control were expanded to five 150 mm plates. Cells were grown to 80% confluency and bait expression was induced with 1 µg/mL of doxycycline supplemented with 50 µM biotin for *in vivo* biotinylation for 24 hours. The media was removed, and cells were washed PBS and flash frozen at -80 °C.

BioID proteomics

Frozen pellets containing induced baits were submitted to the Raught Lab at Princess Margaret Cancer Research Tower (PMCRT), Toronto, Ontario, Canada for processing. Briefly, each pellet is resuspended in 10 mL of modified RIPA lysis buffer (50 mM Tris-HCl pH 7.5, 150 mM NaCl, 1mM EDTA, 1mM EGTA, 1% Triton X-100, 0.1% SDS, 1:500 protease inhibitor cocktail (Sigma-Aldrich), 1:100 Benzonase nuclease

(Sigma-Aldrich) at 4 °C (Coyaud et al . 2015). Cells were lysed by sonication for 30 s at 35 % power. Insoluble material was removed by centrifuging the lysate at 16,000 rpm for 30 min. The clarified supernatant containing the bait protein is then incubated with 30 µL of streptavidin-Sepharose beads (GE) at 4 °C for 3 hr. The beads were washed six times with 50 mM ammonium bicarbonate pH 8.3 to get rid of non-specific binders. Peptides of the bait and prey were generated by TPCK trypsin (Promega) digestion at 37°C for 16 hr. The flow through containing the tryptic peptides were lyophilized and resuspended in 0.1 % formic acid for LC-MS/MS.

Mass spectrometry

LC-MS/MS experimental procedures are taken from Coyaud et al. 2015. LC-MS/MS was conducted using a 120 min reversed-phase buffer gradient running at 250 nl/min (column heated to 40 °C) on a Proxeon EASY-nLC pump in-line with a hybrid LTQ-Orbitrap velos mass spectrometer (Thermo Fisher Scientific). A parent ion scan was performed in the Orbitrap, using a resolving power of 60000. Simultaneously, up to the twenty most intense peaks were selected for MS/MS (minimum ion count of 1000 for activation) using standard CID fragmentation. Fragment ions were detected in the LTQ. Dynamic exclusion was activated such that MS/MS of the same m/z (within a 10-ppm window, exclusion list size 500) detected three times within 45 s were excluded from analysis for 30 s. For protein identification, Proteowizard was used to convert raw files to mzXML and searched using X!Tandem (Craig and Beavis, 2004; Kessner et al., 2008) against Human RefSeq Version 45. Search parameters specified a parent MS tolerance of 15 ppm and an MS/MS fragment ion tolerance of 0.4 Da, with up to two missed cleavages allowed for trypsin. Oxidation of methionine and ubiquitylation of lysine residues were allowed as variable modifications.

Data analysis

The raw data was processed using the CRAPome server (http://crapome.org). Virtual Crapome controls from total HEK293 BirA*-FLAG extracts were used in conjunction with FLAG-BirA*-eGFP as background controls. For SAINTexpress scoring, only the top 6 average controls were considered. The output file was imported to Microsoft Excel for filtering. The filtering scheme involved excluding proteins that had bFDR scores of >0.05 and SAINT scores < 0.8. WT ERG. Associations were then categorized based on molecular function using ShinyGO (http://bioinformatics.sdstate.edu/go/). Evidence for protein associations between the identified interactors were scored using STRING (https://string-db.org/). The combined score involves a weighed combination of the following scores. Co-occurrence score of the phyletic profile derived from similar absence/presence patterns of genes. Co-expression derived from similar patterns of

mRNA expression measured by DNA arrays and similar techniques. Experimental score derived from experimental data such as CoIP, BIND, and IntAct. Data base score derived from curated data from different database such as Biocarta, BioCyc, GO, KEGG and Reactome. Top genes are manually cross referenced with literature.

ERG WT and mutant data sets are combined to assess the changes in the interactome between caused by the mutation. The FCA ratio is calculated as the mutated/WT and ranked as follows: Proteins that score 1.5 ≥ are strongly more abundant in the WT, 1.5 > Protein ≥ 1.2 are mildly more abundant. Proteins with FCA ratios between 1.2 > Protein > 0.8 are considered relatively unchanged. Proteins that scored between 0.8 ≥ Protein > 0.5 are considered mildly loss in the mutant. And proteins that score Proteins ≤ 0.5 are considered strongly loss in the mutant. Significant changes between WT and Mutant associations were quantified using a two tailed distribution with two sample unequal variance (heteroscedastic) t-test. Interaction networks were prepared in Cytoscape.

HDAC3 inhibition in-vitro – differentiation assays and RNA sequencing

For inhibiting HDAC3 in-vitro we used BRD3308 (Sigma, 1639) and RGF966 (Selleck). The inhibitors were dissolved in DMSO according to the manufacture instructions.

Differentiation assays of ER-Hoxb8 cells treated with BRD3308:

In a 24 well plate, 50,000 ER-Hoxb8 cells stably expressing ERG variants were plated after beta-estradiol was washed away from cell culture medium (RPMI supplemented with 10% FBS (Gibco), 1% L-Glutamine, and 1% penicillin/streptomycin, 2% SCF). Cells were treated with either DMSO or BRD3308 in escalating dosage (0, 200, 300, 400, 500, 1000 nM). Following BRD3308 treatment the cells were incubated for 36 hours and the mean fluorescent intensity of Gr1 (APC) was assessed using flow cytometry.

RNA sequencing:

ER-Hoxb8 cells stably expressing ERG variants and an empty vector for control were carefully washed to remove beta-estradiol followed by treatment with either 5μM BRD3308 or DMSO. We conducted four independent experiments for each sample type. The cells were incubated for 36 hours and fluidized in TRIzol reagent and prepared for RNA sequencing as described above. Data analysis was conducted as described for murine fetal liver derived HSPC.

CRISPR-Cas9 mediated targeting of ERG in leukemic cell lines

Cloning and virus preparation of single guide RNA

Single guide RNA (sgRNA) against human *ERG* was cloned into CRISPR V2 plasmid (addgene, #52961). Three million HEK 293T cells were seeded per plate of 100mm dish. Total 10 dishes were used for per guide of human ERG. Three sgRNAs were chosen (see below): two targeting exon 2 while one targets exon 5 (Thirant et al., 2017). The transfection of 293T cells was performed using calcium chloride transfection based on the manufacturer's instructions. The virus was collected twice after 48 and 78 hours. The virus was then filtered through a 0.2mM filter. To achieve the final concentration of 10%, 10ml of PEG8000 (40%) was added to 30ml of virus. After being added to PEG 8000, the virus was kept overnight at -20°C. The next day, the virus was thawed at room temperature and centrifuged for 15 minutes at 4000 rpm using a swigging bucket centrifuge. After discarding the supernatant, the virus (30ml) was resuspended in 200l, aliquoted, and stored at -80°C for future use.

ERG targeting guides	Sequence	Position	PAM
Guide1	GTGGGCAGCCCAGACACCGT	Exon 5	TGG
Guide2	GTCCTCACTCACAACTGATA	Exon 2	AGG
Guide3	AGCCTTATCAGTTGTGAGTG	Exon 2	AGG

KO of *ERG* in leukemic cell lines

Each well of a 12-well plate was seeded with 1 million cells and polybrene was added at a final concentration of 6µg/ml. Cells were kept at 37°C in presence of 5% Co2 for 30 mins. Thereafter, the *ERG*-targeting Guide RNA 1, 2 and 3 were pooled with a nontargeting Guide virus. A total of 100µl of pooled Erg virus and Non-targeting guide RNA virus was added to the cells. Spinfection was performed by spinning plates at a speed of 1000g at 32°C for 90 minutes. The cells were kept at 37°C with 5% carbon

dioxide after spinfection. Approximately 24 hours after transduction, puromycin was added at a final concentration of 1µg/ml.

Apoptosis analysis

Cells were seeded at 20,000 per well of a 48-well plate after 2 days of puromycin selection. Cells were harvested for annexin-7AA staining every 4 days. Harvested cells were centrifuged at 300g for 5 minutes at 4°C, then washed with PBS. After discarding the supernatant, cells were stained with 100µl Annexin-APC antibody diluted in Annexin buffer (1:20 dilution). Cells were kept in darkness at room temperature for 30 minutes. The cells were then washed with PBS and centrifuged. The supernatant was discarded, and the cells were suspended in staining media (PBS + 2% FBS) with 7AAD (a dilution of 1:100). Flow cytometry was used to analyze the cells after 5 minutes incubation.

HDAC3 inhibition and CRISPR targeting of HDAC3 in vivo

HDAC3 inhibition using RGF966 in NSG mice

Busulfan (20mg/kg) was administered intravenous to NSG mice 24 hours prior to transplantation. SKNO1 cells (250K) were transplanted through the tail veins of 24 NSG mice (12 from each group – vehicle vs RFGP966). One day following transplantation, mice were treated intraperitoneally with either 15mg/kg of RGFP966 or vehicle once daily for 21 days. The mice were then sacrificed, and the bone marrow was analyzed for human CD45 to assess disease burden.

RGFP966 (Selleck) was dissolved in DMSO (final concentration – 7%), PEG300 (40%), Tween 80 (10%) and 0.9 % w/v NaCl (43%). A similar concentration of ingredients was used for the vehicle.

Targeting HDAC3 using CRISPR-dCas9 system in SKNO1 cells

CRISPR-dCas9 system was used to inhibit HDAC3 expression in SKNO1 cells. Monoclonal SKNO1 dCas9 cells were generated by transduction with a dCas9 lentivirus. Transduced cells were selected by adding

blasticidin at 1mg/ml final concentration. Single cells were seeded per well of a 96 well plate. To test the efficiency of clones, we transduced single cells with RFP virus which contained a guide RNA (sgRNA) that targeted the RFP in the original vector itself. In flow cytometry, selected clones exhibited an 85-89% reduction in RFP MFI (mean fluorescent intensity). Selected SKNO1 dCas9 monoclonal cells were later transduced with lentivirus containing sgRNA targeting the transcription start site of the HDAC3 gene. Transduced SKNO1 dCas9 cells were selected by adding puromycin to the media at final concentration of 1µg/ml. Cells were maintained in puromycin for 14 days, and the expression of HDAC3 was measured at the RNA and protein levels (figure S8).

Once HDAC3 inhibition was confirmed, 250k sgNT-SKNO1 (non-targeting) dCas9 cells and sgHDAC3-SKNO1 dCas9 cells were transplanted per mouse. Mice were sacrificed 45 days after transplantation. The bone marrow cells were harvested and stained with an anti-hCD45 antibody to determine disease burden. Same procedure was conducted for targeting HDAC3 in THP1 cells.

HDAC3 targeting guides	Sequence
Guide1	CGGCACCATGGCCAAGACCG
Guide2	GTAGAAATAGGCCACGGTCT
Guide3	ATAGGCCACGGTCTTGGCCA

References

1. Leprince D, Gegonne A, Coll J, et al. A putative second cell-derived oncogene of the avian leukaemia retrovirus E26. *Nature*. Nov 24-30 1983;306(5941):395-7. doi:10.1038/306395a0

2. Nunn MF, Seeburg PH, Moscovici C, Duesberg PH. Tripartite structure of the avian erythroblastosis virus E26 transforming gene. *Nature*. Nov 24-30 1983;306(5941):391-5. doi:10.1038/306391a0

3. Malinge S, Izraeli S, Crispino JD. Insights into the manifestations, outcomes, and mechanisms of leukemogenesis in Down syndrome. *Blood*. Mar 19 2009;113(12):2619-28.

4. Rao VN, Papas TS, Reddy ES. erg, a human ets-related gene on chromosome 21: alternative splicing, polyadenylation, and translation. *Science*. Aug 7 1987;237(4815):635-9.

5. Loughran SJ, Kruse EA, Hacking DF, et al. The transcription factor Erg is essential for definitive hematopoiesis and the function of adult hematopoietic stem cells. *Nat Immunol*. Jul 2008;9(7):810-9.

6. Taoudi S, Bee T, Hilton A, et al. ERG dependence distinguishes developmental control of hematopoietic stem cell maintenance from hematopoietic specification. *Genes Dev*. Feb 1 2011;25(3):251-62. doi:10.1101/gad.2009211

7. Knudsen KJ, Rehn M, Hasemann MS, et al. ERG promotes the maintenance of hematopoietic stem cells by restricting their differentiation. *Genes Dev*. Sep 15 2015;29(18):1915-29. doi:10.1101/gad.268409.115

8. Wilson NK, Foster SD, Wang X, et al. Combinatorial transcriptional control in blood stem/progenitor cells: genome-wide analysis of ten major transcriptional regulators. *Cell Stem Cell*. Oct 8 2010;7(4):532-44. doi:S1934-5909(10)00440-6 [pii]10.1016/j.stem.2010.07.016

9. Pimkin M, Kossenkov AV, Mishra T, et al. Divergent functions of hematopoietic transcription factors in lineage priming and differentiation during erythro-megakaryopoiesis. *Genome Res*. Dec 2014;24(12):1932-44. doi:10.1101/gr.164178.113

10. Beck D, Thoms JA, Perera D, et al. Genome-wide analysis of transcriptional regulators in human HSPCs reveals a densely interconnected network of coding and noncoding genes. *Blood*. Oct 3 2013;122(14):e12-22. doi:10.1182/blood-2013-03-490425

11. Marcucci G, Baldus CD, Ruppert AS, et al. Overexpression of the ETS-related gene, ERG, predicts a worse outcome in acute myeloid leukemia with normal karyotype: a Cancer and Leukemia Group B study. *J Clin Oncol*. Dec 20 2005;23(36):9234-42.

12. Metzeler KH, Dufour A, Benthaus T, et al. ERG expression is an independent prognostic factor and allows refined risk stratification in cytogenetically normal acute myeloid leukemia: a comprehensive analysis of ERG, MN1, and BAALC transcript levels using oligonucleotide microarrays. *J Clin Oncol*. Oct 20 2009;27(30):5031-8. doi:10.1200/JCO.2008.20.5328

13. Goldberg L, Tijssen MR, Birger Y, et al. Genome-scale expression and transcription factor binding profiles reveal therapeutic targets in transgenic ERG myeloid leukemia. *Blood*. Oct 10 2013;122(15):2694-703. doi:10.1182/blood-2013-01-477133

14. Thoms JA, Birger Y, Foster S, et al. ERG promotes T-acute lymphoblastic leukemia and is transcriptionally regulated in leukemic cells by a stem cell enhancer. *Blood*. Jun 30 2011;117(26):7079-89. doi:10.1182/blood-2010-12-317990

15. Fukushima Y, Fujii N, Tabata Y, et al. [AML(M7) associated with t(16;21)(p11;q22) showing relapse after unrelated bone marrow transplantation and disappearance of TLS/FUS-ERG mRNA]. *Rinsho Ketsueki*. Jun 2001;42(6):502-6.

16. Panagopoulos I, Gorunova L, Zeller B, Tierens A, Heim S. Cryptic FUS-ERG fusion identified by RNA-sequencing in childhood acute myeloid leukemia. *Oncol Rep*. Dec 2013;30(6):2587-92. doi:10.3892/or.2013.2751

17. Zhang J, McCastlain K, Yoshihara H, et al. Deregulation of DUX4 and ERG in acute lymphoblastic leukemia. *Nat Genet*. Dec 2016;48(12):1481-1489. doi:10.1038/ng.3691

18. Zaliova M, Potuckova E, Hovorkova L, et al. ERG deletions in childhood acute lymphoblastic leukemia with DUX4 rearrangements are mostly polyclonal, prognostically relevant and their detection rate strongly depends on screening method sensitivity. *Haematologica*. Jul 2019;104(7):1407-1416. doi:10.3324/haematol.2018.204487

19. Rainis L, Toki T, Pimanda JE, et al. The proto-oncogene ERG in megakaryoblastic leukemias. *Cancer Res*. Sep 1 2005;65(17):7596-602. doi:10.1158/0008-5472.CAN-05-0147

20. Birger Y, Goldberg L, Chlon TM, et al. Perturbation of fetal hematopoiesis in a mouse model of Down syndrome's transient myeloproliferative disorder. *Blood*. Aug 8 2013;122(6):988-98. doi:10.1182/blood-2012-10-460998

21. Stankiewicz MJ, Crispino JD. ETS2 and ERG promote megakaryopoiesis and synergize with alterations in GATA-1 to immortalize hematopoietic progenitor cells. *Blood*. Apr 2 2009;113(14):3337-47. doi:10.1182/blood-2008-08-174813

22. Salek-Ardakani S, Smooha G, de Boer J, et al. ERG is a megakaryocytic oncogene. *Cancer Res*. Jun 1 2009;69(11):4665-73. doi:10.1158/0008-5472.CAN-09-0075

23. Wang X, Crispino JD, Letting DL, Nakazawa M, Poncz M, Blobel GA. Control of megakaryocyte-specific gene expression by GATA-1 and FOG-1: role of Ets transcription factors. *EMBO J*. Oct 1 2002;21(19):5225-34. doi:10.1093/emboj/cdf527

24. Thirant C, Ignacimouttou C, Lopez CK, et al. ETO2-GLIS2 Hijacks Transcriptional Complexes to Drive Cellular Identity and Self-Renewal in Pediatric Acute Megakaryoblastic Leukemia. *Cancer Cell*. Mar 13 2017;31(3):452-465. doi:10.1016/j.ccell.2017.02.006

25. Mandoli A, Singh AA, Prange KHM, et al. The Hematopoietic Transcription Factors RUNX1 and ERG Prevent AML1-ETO Oncogene Overexpression and Onset of the Apoptosis Program in t(8;21) AMLs. *Cell Rep*. Nov 15 2016;17(8):2087-2100. doi:10.1016/j.celrep.2016.08.082

26. Huang Y, Mouttet B, Warnatz HJ, et al. The Leukemogenic TCF3-HLF Complex Rewires Enhancers Driving Cellular Identity and Self-Renewal Conferring EP300 Vulnerability. *Cancer Cell*. Dec 9 2019;36(6):630-644 e9. doi:10.1016/j.ccell.2019.10.004

27. Tursky ML, Beck D, Thoms JA, et al. Overexpression of ERG in cord blood progenitors promotes expansion and recapitulates molecular signatures of high ERG leukemias. *Leukemia*. Apr 2015;29(4):819-

27. doi:10.1038/leu.2014.299

28. Rieger MA, Smejkal BM, Schroeder T. Improved prospective identification of megakaryocyte-erythrocyte progenitor cells. *Br J Haematol*. Feb 2009;144(3):448-51. doi:10.1111/j.1365-2141.2008.07419.x

29. Wang GG, Pasillas MP, Kamps MP. Persistent transactivation by meis1 replaces hox function in myeloid leukemogenesis models: evidence for co-occupancy of meis1-pbx and hox-pbx complexes on promoters of leukemia-associated genes. *Mol Cell Biol*. May 2006;26(10):3902-16. doi:10.1128/MCB.26.10.3902-3916.2006

30. Sun Y, Zhou B, Mao F, et al. HOXA9 Reprograms the Enhancer Landscape to Promote Leukemogenesis. *Cancer Cell*. Oct 8 2018;34(4):643-658 e5. doi:10.1016/j.ccell.2018.08.018

31. Yokoyama T, Nakatake M, Kuwata T, et al. MEIS1-mediated transactivation of synaptotagmin-like 1 promotes CXCL12/CXCR4 signaling and leukemogenesis. *J Clin Invest*. May 2 2016;126(5):1664-78. doi:10.1172/JCI81516

32. Argiropoulos B, Yung E, Humphries RK. Unraveling the crucial roles of Meis1 in leukemogenesis and normal hematopoiesis. *Genes Dev*. Nov 15 2007;21(22):2845-9. doi:10.1101/gad.1619407

33. Steinauer N, Guo C, Zhang J. Emerging Roles of MTG16 in Cell-Fate Control of Hematopoietic Stem Cells and Cancer. *Stem Cells Int*. 2017;2017:6301385. doi:10.1155/2017/6301385

34. Fischer MA, Moreno-Miralles I, Hunt A, Chyla BJ, Hiebert SW. Myeloid translocation gene 16 is required for maintenance of haematopoietic stem cell quiescence. *EMBO J*. Mar 21 2012;31(6):1494-505. doi:10.1038/emboj.2011.500

35. Denay G, Vachon G, Dumas R, Zubieta C, Parcy F. Plant SAM-Domain Proteins Start to Reveal Their Roles. *Trends Plant Sci*. Aug 2017;22(8):718-725. doi:10.1016/j.tplants.2017.06.006

36. Johnson PE, Donaldson LW. RNA recognition by the Vts1p SAM domain. *Nat Struct Mol Biol*. Feb 2006;13(2):177-8. doi:10.1038/nsmb1039

37. Rothe B, Leal-Esteban L, Bernet F, et al. Bicc1 Polymerization Regulates the Localization and Silencing of Bound mRNA. *Mol Cell Biol*. Oct 2015;35(19):3339-53. doi:10.1128/MCB.00341-15

38. Roux KJ, Kim DI, Raida M, Burke B. A promiscuous biotin ligase fusion protein identifies proximal and interacting proteins in mammalian cells. *J Cell Biol*. Mar 19 2012;196(6):801-10. doi:10.1083/jcb.201112098

39. Mellacheruvu D, Wright Z, Couzens AL, et al. The CRAPome: a contaminant repository for affinity purification-mass spectrometry data. *Nat Methods*. Aug 2013;10(8):730-6. doi:10.1038/nmeth.2557

40. Sandoval GJ, Pulice JL, Pakula H, et al. Binding of TMPRSS2-ERG to BAF Chromatin Remodeling Complexes Mediates Prostate Oncogenesis. *Mol Cell*. Aug 16 2018;71(4):554-566 e7. doi:10.1016/j.molcel.2018.06.040

41. Wang GG, Calvo KR, Pasillas MP, Sykes DB, Hacker H, Kamps MP. Quantitative production of macrophages or neutrophils ex vivo using conditional Hoxb8. *Nat Methods*. Apr 2006;3(4):287-93. doi:10.1038/nmeth865

42. Wagner FF, Lundh M, Kaya T, et al. An Isochemogenic Set of Inhibitors To Define the Therapeutic Potential of Histone Deacetylases in beta-Cell Protection. *ACS Chem Biol*. Feb 19 2016;11(2):363-74. doi:10.1021/acschembio.5b00640

43. Long J, Fang WY, Chang L, et al. Targeting HDAC3, a new partner protein of AKT in the reversal of chemoresistance in acute myeloid leukemia via DNA damage response. *Leukemia*. Dec 2017;31(12):2761-2770. doi:10.1038/leu.2017.130

44. Yassin M, Aqaqe N, Yassin AA, et al. A novel method for detecting the cellular stemness state in normal and leukemic human hematopoietic cells can predict disease outcome and drug sensitivity. *Leukemia*. Aug 2019;33(8):2061-2077. doi:10.1038/s41375-019-0386-z

45. Summers AR, Fischer MA, Stengel KR, et al. HDAC3 is essential for DNA replication in hematopoietic progenitor cells. *J Clin Invest*. Jul 2013;123(7):3112-23. doi:10.1172/JCI60806

46. Stadhouders R, Cico A, Stephen T, et al. Control of developmentally primed erythroid genes by combinatorial co-repressor actions. *Nat Commun*. Nov 23 2015;6:8893. doi:10.1038/ncomms9893

47. Guo X, Plank-Bazinet J, Krivega I, Dale RK, Dean A. Embryonic erythropoiesis and hemoglobin switching require transcriptional repressor ETO2 to modulate chromatin organization. *Nucleic Acids Res*. Oct 9 2020;48(18):10226-10240. doi:10.1093/nar/gkaa736

48. Lausen J, Cho S, Liu S, Werner MH. The nuclear receptor co-repressor (N-CoR) utilizes repression domains I and III for interaction and co-repression with ETO. *J Biol Chem*. Nov 19 2004;279(47):49281-8. doi:10.1074/jbc.M407239200

49. Chng KR, Chang CW, Tan SK, et al. A transcriptional repressor co-regulatory network governing androgen response in prostate cancers. *The EMBO journal*. Jun 13 2012;31(12):2810-23. doi:emboj2012112 [pii]

10.1038/emboj.2012.112

50. Bjorkman M, Iljin K, Halonen P, et al. Defining the molecular action of HDAC inhibitors and synergism with androgen deprivation in ERG-positive prostate cancer. *Int J Cancer*. Dec 15 2008;123(12):2774-81. doi:10.1002/ijc.23885

51. Antoniani C, Romano O, Miccio A. Concise Review: Epigenetic Regulation of Hematopoiesis: Biological Insights and Therapeutic Applications. *Stem Cells Transl Med*. Dec 2017;6(12):2106-2114. doi:10.1002/sctm.17-0192

52. Calo E, Wysocka J. Modification of enhancer chromatin: what, how, and why? *Mol Cell*. Mar 7 2013;49(5):825-37. doi:10.1016/j.molcel.2013.01.038

53. Lara-Astiaso D, Weiner A, Lorenzo-Vivas E, et al. Immunogenetics. Chromatin state dynamics during blood formation. *Science*. Aug 22 2014;345(6199):943-9. doi:10.1126/science.1256271

54. Yu X, Wu C, Bhavanasi D, Wang H, Gregory BD, Huang J. Chromatin dynamics during the differentiation of long-term hematopoietic stem cells to multipotent progenitors. *Blood Adv*. Jun 13 2017;1(14):887-898. doi:10.1182/bloodadvances.2016003384

55. Thoms JAI, Truong P, Subramanian S, et al. Disruption of a GATA2, TAL1, ERG regulatory circuit promotes erythroid transition in healthy and leukemic stem cells. *Blood*. Jun 1 2021;doi:10.1182/blood.2020009707

56. Grimwade D, Hills RK, Moorman AV, et al. Refinement of cytogenetic classification in acute myeloid leukemia: determination of prognostic significance of rare recurring chromosomal abnormalities among 5876 younger adult patients treated in the United Kingdom Medical Research Council trials. *Blood*. Jul 22 2010;116(3):354-65. doi:10.1182/blood-2009-11-254441

57. Davis JN, McGhee L, Meyers S. The ETO (MTG8) gene family. *Gene*. Jan 16 2003;303:1-10. doi:10.1016/s0378-1119(02)01172-1

58. Wang J, Hoshino T, Redner RL, Kajigaya S, Liu JM. ETO, fusion partner in t(8;21) acute myeloid leukemia, represses transcription by interaction with the human N-CoR/mSin3/HDAC1 complex. *Proc Natl Acad Sci U S A*. Sep 1 1998;95(18):10860-5. doi:10.1073/pnas.95.18.10860

59. Meyers S, Lenny N, Hiebert SW. The t(8;21) fusion protein interferes with AML-1B-dependent transcriptional activation. *Mol Cell Biol*. Apr 1995;15(4):1974-82. doi:10.1128/MCB.15.4.1974

60. Okuda T, Cai Z, Yang S, et al. Expression of a knocked-in AML1-ETO leukemia gene inhibits the establishment of normal definitive hematopoiesis and directly generates dysplastic hematopoietic progenitors. *Blood*. May 1 1998;91(9):3134-43.

61. Yergeau DA, Hetherington CJ, Wang Q, et al. Embryonic lethality and impairment of haematopoiesis in mice heterozygous for an AML1-ETO fusion gene. *Nat Genet*. Mar 1997;15(3):303-6. doi:10.1038/ng0397-303

62. Guo C, Li J, Steinauer N, et al. Histone deacetylase 3 preferentially binds and collaborates with the transcription factor RUNX1 to repress AML1-ETO-dependent transcription in t(8;21) AML. *J Biol Chem*. Mar 27 2020;295(13):4212-4223. doi:10.1074/jbc.RA119.010707

63. Richon VM, Emiliani S, Verdin E, et al. A class of hybrid polar inducers of transformed cell differentiation inhibits histone deacetylases. *Proc Natl Acad Sci U S A*. Mar 17 1998;95(6):3003-7. doi:10.1073/pnas.95.6.3003

64. Quintas-Cardama A, Santos FP, Garcia-Manero G. Histone deacetylase inhibitors for the treatment of myelodysplastic syndrome and acute myeloid leukemia. *Leukemia*. Feb 2011;25(2):226-35. doi:10.1038/leu.2010.276

65. Garcia-Manero G, Yang H, Bueso-Ramos C, et al. Phase 1 study of the histone deacetylase inhibitor vorinostat (suberoylanilide hydroxamic acid [SAHA]) in patients with advanced leukemias and myelodysplastic syndromes. *Blood*. Feb 1 2008;111(3):1060-6. doi:10.1182/blood-2007-06-098061

66. Kuendgen A, Schmid M, Schlenk R, et al. The histone deacetylase (HDAC) inhibitor valproic acid as monotherapy or in combination with all-trans retinoic acid in patients with acute myeloid leukemia. *Cancer*. Jan 1 2006;106(1):112-9. doi:10.1002/cncr.21552

67. Amendola M, Venneri MA, Biffi A, Vigna E, Naldini L. Coordinate dual-gene transgenesis by lentiviral vectors carrying synthetic bidirectional promoters. *Nat Biotechnol*. Jan 2005;23(1):108-16. doi:10.1038/nbt1049

68. Love MI, Huber W, Anders S. Moderated estimation of fold change and dispersion for RNA-seq data with DESeq2. *Genome Biol*. 2014;15(12):550. doi:10.1186/s13059-014-0550-8

69. Subramanian A, Tamayo P, Mootha VK, et al. Gene set enrichment analysis: a knowledge-based approach for interpreting genome-wide expression profiles. *Proc Natl Acad Sci U S A*. Oct 25 2005;102(43):15545-50. doi:10.1073/pnas.0506580102

70. Yu G, Wang LG, Han Y, He QY. clusterProfiler: an R package for comparing biological themes among gene clusters. *OMICS*. May 2012;16(5):284-7. doi:10.1089/omi.2011.0118

71. Raudvere U, Kolberg L, Kuzmin I, et al. g:Profiler: a web server for functional enrichment analysis and conversions of gene lists (2019 update). *Nucleic Acids Res*. Jul 2 2019;47(W1):W191-W198. doi:10.1093/nar/gkz369

72. Akalin A, Franke V, Vlahovicek K, Mason CE, Schubeler D. Genomation: a toolkit to summarize, annotate and visualize genomic intervals. *Bioinformatics*. Apr 1 2015;31(7):1127-9. doi:10.1093/bioinformatics/btu775

Figures

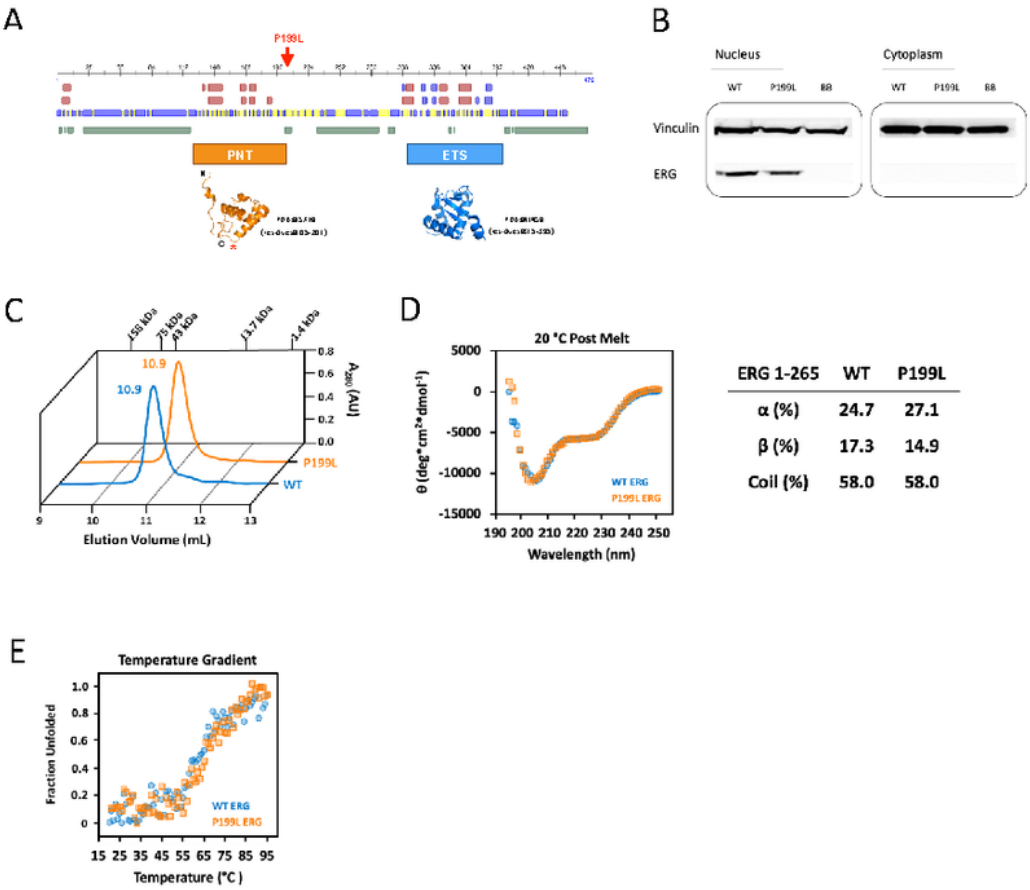

ERG 1-265	WT	P199L
α (%)	24.7	27.1
β (%)	17.3	14.9
Coil (%)	58.0	58.0

Figure 1

Figure 1

P199L does not significantly affect the secondary structure or thermal stability of ERG.

A. Sequence-based predictions of ERG, including secondary structure (red: helix, blue: beta strand), solvent exposure (blue: exposed, yellow: buried), and disorder (green) (http://www.predictprotein,org). Experimentally determined structures of the ordered domains are also shown. Proline 199 is the last amino acid of the PNT domain.

B. Immunoblot for FLAG in the nuclear and cytoplasmic fractions of CMK cells transduced with ERG variants.

C. Analytical size exclusion chromatogram of the ERG constructs. Protein size standards are indicated.

D. Circular dichroism spectrum scan at 20 °C post-melt.

E. Circular dichroism spectrum collected at 226 nm in a temperature gradient.

WT – Wild type ERG, BB – Backbone.

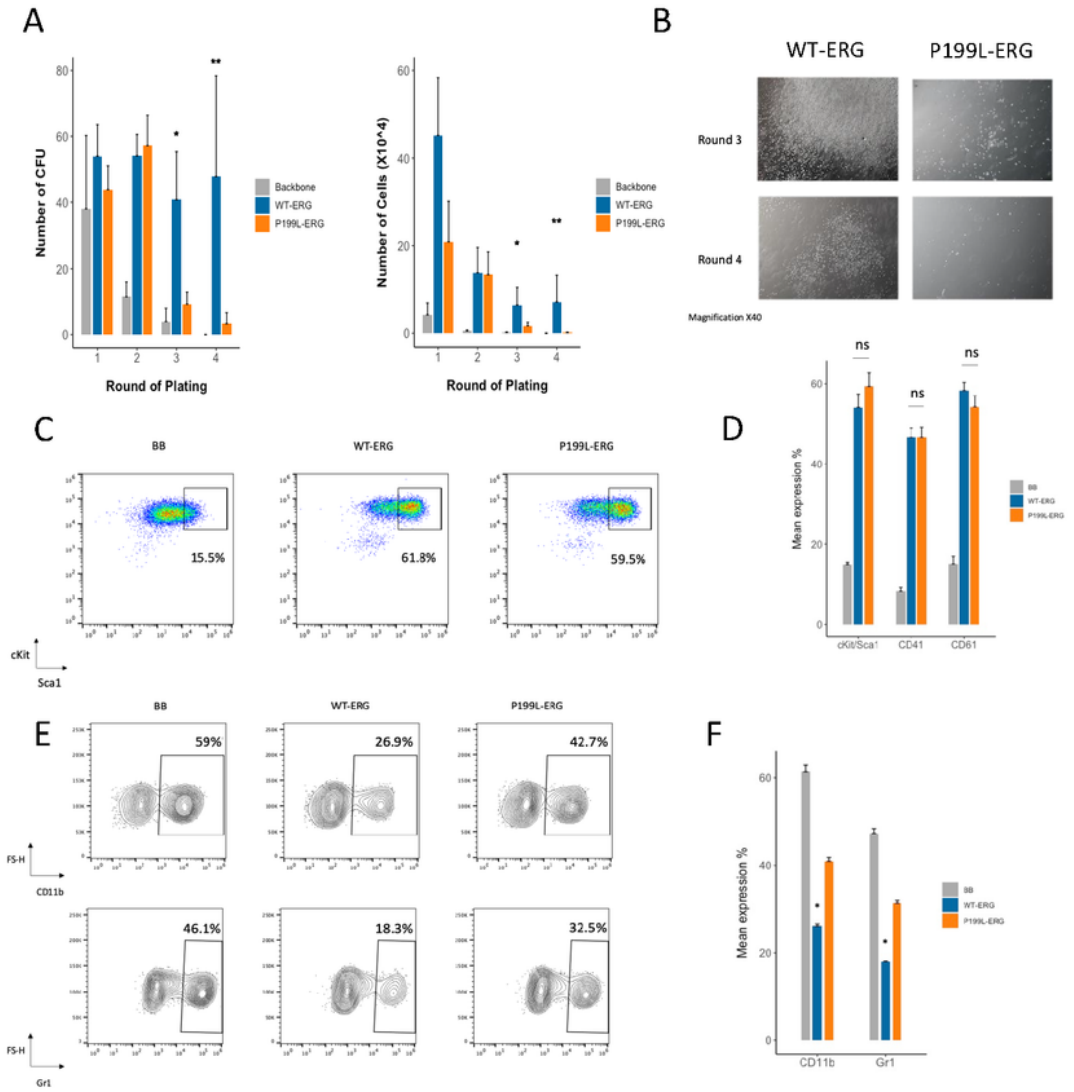

Figure 2

Figure 2

P199L alleviates the effect of ERG forced expression on self-renewal and myeloid differentiation of HSPC.

A. Re-plating assay in semi-solid conditions of murine fetal liver derived HSPC transduced with ERG variants. The number of CFU (left panel) and total number of cells collected (right panel) per 10^4 cells plated is presented for each round of plating (n=4, Data are represented as mean ± SEM, Kruskal Wallis rank-sum test)

B. Microscopic view of colonies morphology between groups. MagnificationX40.

C. Representative flow cytometry analysis of murine HSPC (c-Kit, Sca1) cell surface markers.

D. Summary bar graphs of flow cytometry analysis for the end of round one (n=4, Data are represented as mean ± SEM).

E. Representative flow cytometry analysis of myeloid differentiation using measurements for cell surface expression of CD11b and Gr-1 in fetal-liver derived HSPC transduced with ERG variants.

F. Summary bar graphs of flow cytometry analysis (right panel, n=3, Kruskal-Wallis rank sum test was used for p value calculation and Wilcoxon rank sum test was used for post-hoc analysis).

CFU – Colony forming units, * denotes $P<0.05$. ** denotes $P<0.01$.

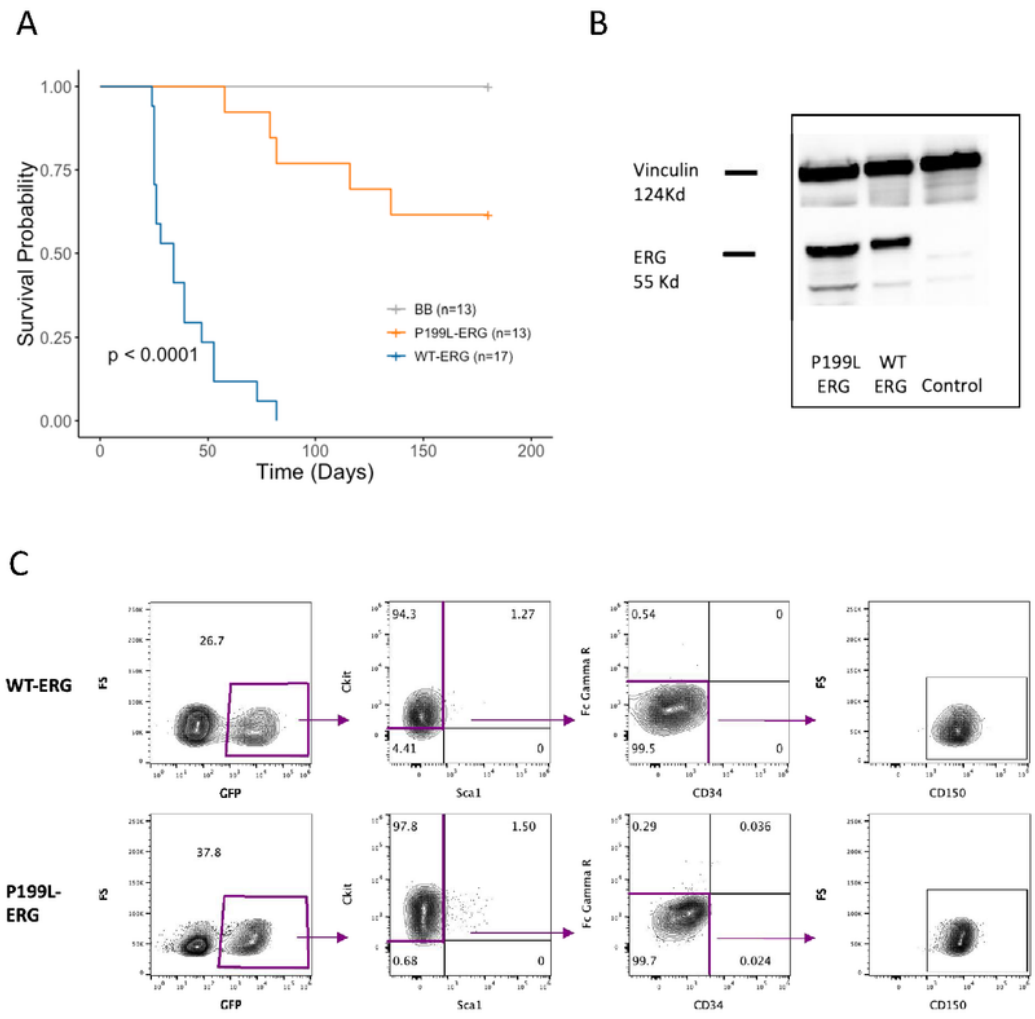

Figure 3

Figure 3

P199L severely disrupts ERG transforming capacity in-vivo.

A. Survival analysis of C57B/6 mice transplanted with murine fetal liver derived HSPC following transduction with ERG variants (10^5 transduced cells/mouse). A log-rank test was used to compare survival distribution between groups.

B. Immunoblot of HA tagged ERG to compare the levels of protein expression of WT and mutated ERG in the spleen of leukemic mice.

C. Immunophenotype of AML blasts (GFP+) from the bone marrow of leukemic mice.

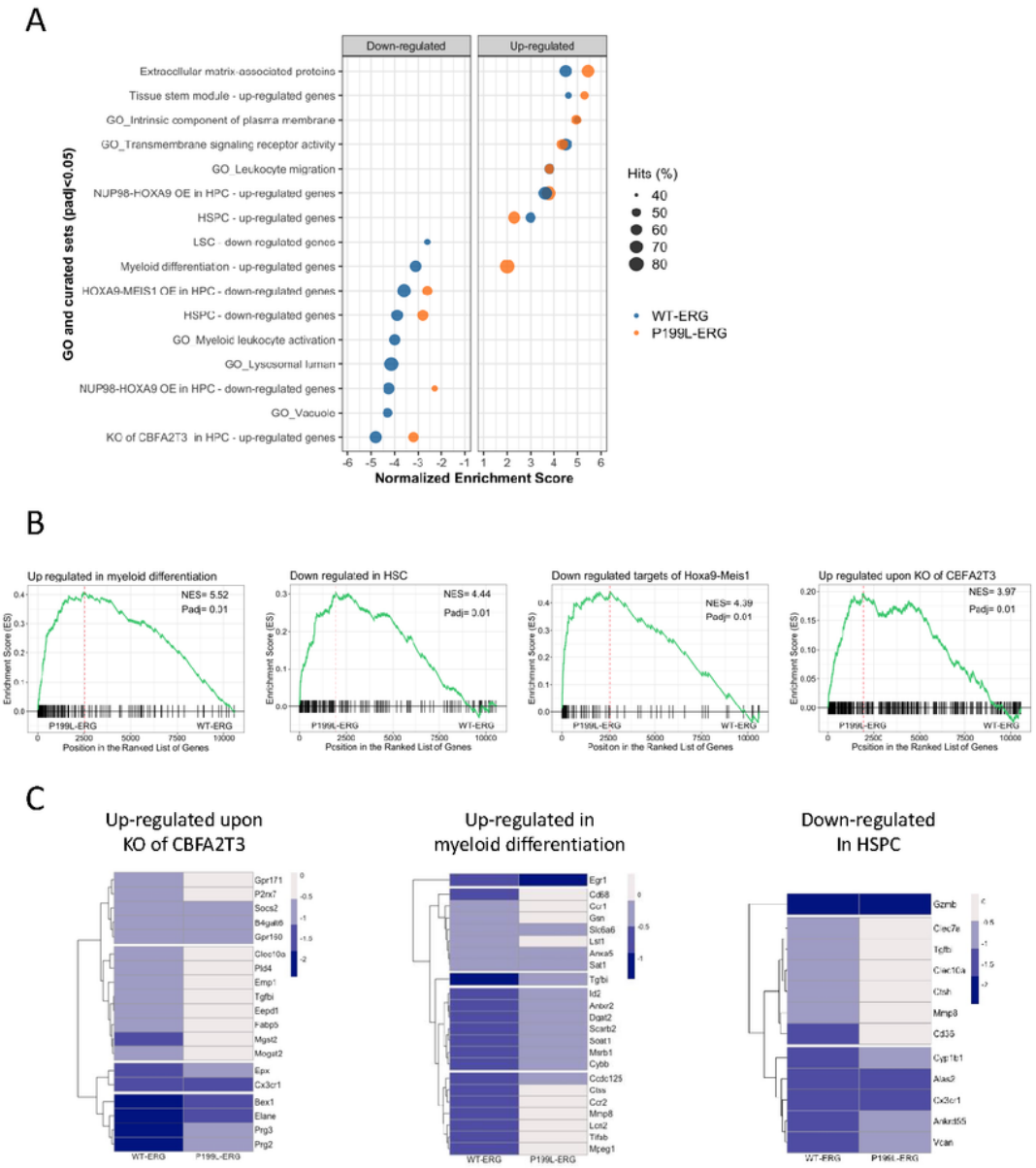

Figure 4

Figure 4

P199L impedes ERG-mediated transcriptional gene repression in HSPC.

A. Pathway and functional analysis of the gene expression profile of ERG variants against BB was performed using GSEA. Molecular pathways related to down and up-regulated genes are presented separately. The absence of a circle implies no statistical significance enrichment for a particular gene

set. A positive enrichment score refers to up-regulated genes, and a negative score refers to down-regulated genes (ERG variants against the backbone). The percentage of hits (“tags” in leading-edge analysis) is displayed to indicate the percentage of genes contributing to the enrichment score for each set of genes.

B. GSEA of upregulated genes (P199L-ERG against WT-ERG).

C. Most significant DEG (padj<0.05) contributing to the enrichment scores in A are shown for representative sets (ERG variants against BB).

HSPC – hematopoietic stem and progenitor cells, LSC – leukemic stem cells. NES – Normalized enrichment score. DEG – differentially expressed genes. BB – backbone.

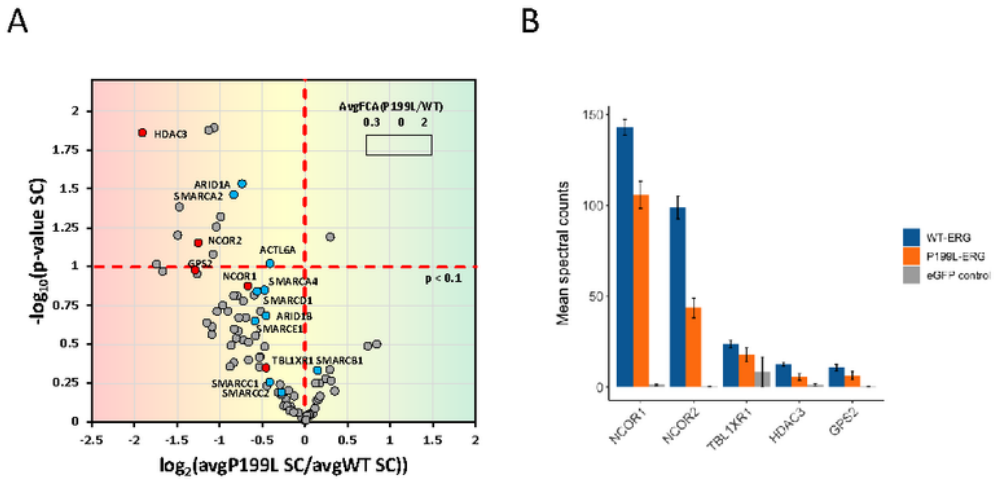

Figure 5

Figure 5

P199L disrupts the interaction of ERG with chromatin modifiers.

A. Volcano plot comparing the spectral counts of identified interactors between

FLAG-BirA-ERG WT and P199L. The background color indicates the prey FCA P199L/WT ratio. Significant proteins were selected with a p < 0.08 cut off based on spectral counts ratios. Notable proteins are colored according to molecular function.

B. Mean spectral counts for NCOR-HDAC3 hits (averaged between two biological replicates).

Saint scores and bFDR are > 0.8 and < 0.05 respectively. FCA – Fold change. SC – Spectral counts.

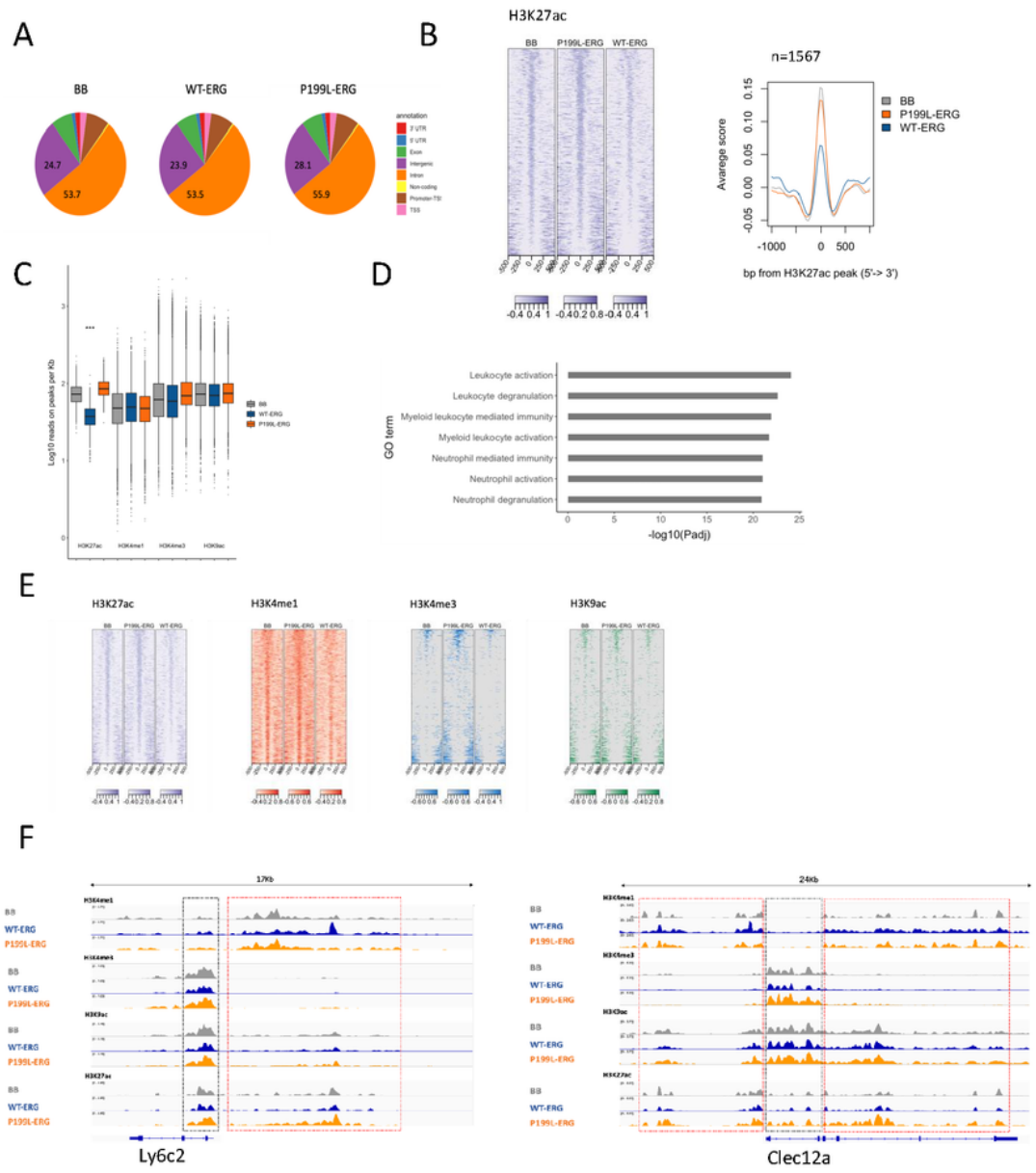

Figure 6

Figure 6

ERG affects chromatin modifications at myeloid related gene loci.

A. Global annotation statistics on the enrichment of ChIP signal of H3K27ac across groups.

B. Heatmap hierarchical clustering (left panel) and metagene plots (right panel) showing H3K27ac peaks of down-regulated and hypoacetylated DEG following expression of WT-ERG force in Hoxb8 cells.

C. The intensity signal of normalized read counts of histone peaks is presented for genes identified in B (unpaired Wilcoxson test, P-value = 2.2X10-16).

D. GO analysis based on the nearest transcription start site to peaks identified in B.

Adjusted p values are displayed.

E. Heatmap hierarchical clustering centered on H3K27ac peaks associated with genes identified in B. The co-occupancy for H3K4me1, H3K4me3 and H3K9ac marks is shown.

F. Track example for two genes identified in B and D - Ly6c2 (Gr1) and Clec12a. Dashed black boxes indicate regions of H3K4me1 and H3K27ac overlap, and dashed red boxes indicate regions that relate to the transcription start site (H3K4me3, H3K9ac, and H3K27ac overlap).

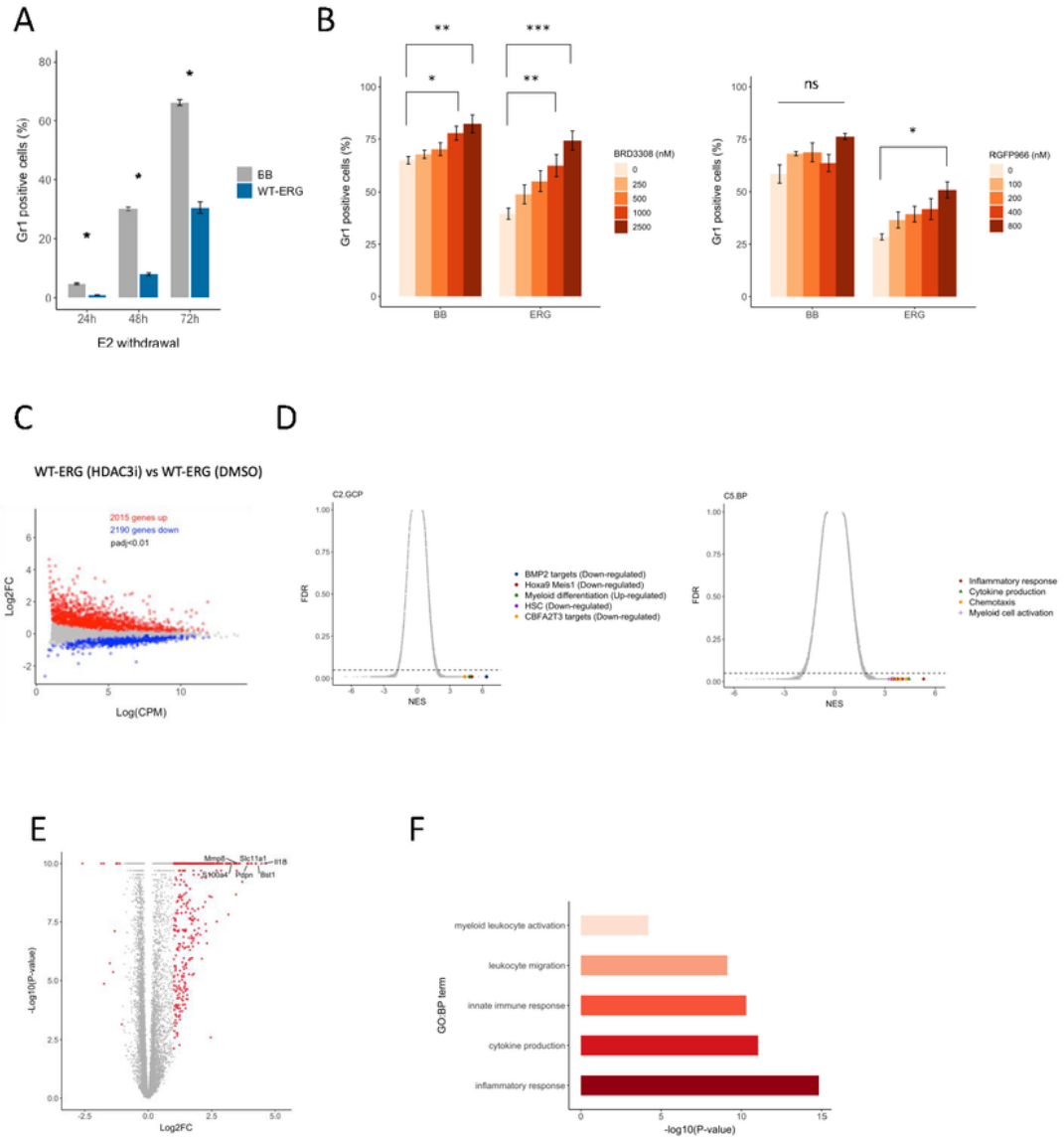

Figure 7

Figure 7

HDAC3 inhibition alleviates the myeloid differentiation block induced by ERG forced expression in hematopoietic progenitor cells.

A. Analysis of myeloid differentiation in human ERG expressing ER-Hoxb8 cells. GR-1 percentage was measured using flow cytometry after withdrawal of beta estradiol (E2). Wilcoxon test, P=0.0287 for each time point.

B. Analysis of myeloid differentiation of ER-Hoxb8 cells expressing human ERG following inhibition of HDAC3 with BRD3308 (left panel) and RGFP966 (right panel). One-way ANOVA and Kruskal Wallis test (BRD3308 and RGFP966 respectively).

C. RNA sequencing in human ERG-expressing ER-Hoxb8 cells treated with either DMSO or 2.5μM BRD3308. A MA-plot illustrates the effect of BRD3308 treatment on gene expression. Differentially expressed genes (Padj<0.05) are indicated.

D. GSEA of genetic and chemical perturbation (C2.CGP) and gene ontology biological process gene sets (C5.BP) following HDAC3 inhibition in human ERG expressing ER-Hoxb8 cells. Most significant up-regulated gene sets are indicated.

E. Most significant differentially expressed genes following HDAC3 inhibition in human ERG expressing ER-Hoxb8 cells. Genes in red indicate log2 fold change > 1 and < -1 and FDR < 0.01.

F. Gene Ontology on differentially expressed genes presented in E.

CPM – counts per million. NES – Normalized enrichment score. FDR – false discovery rate. * p<0.05, ** p<0.01, *** p<0.001, ns – nonsignificant.

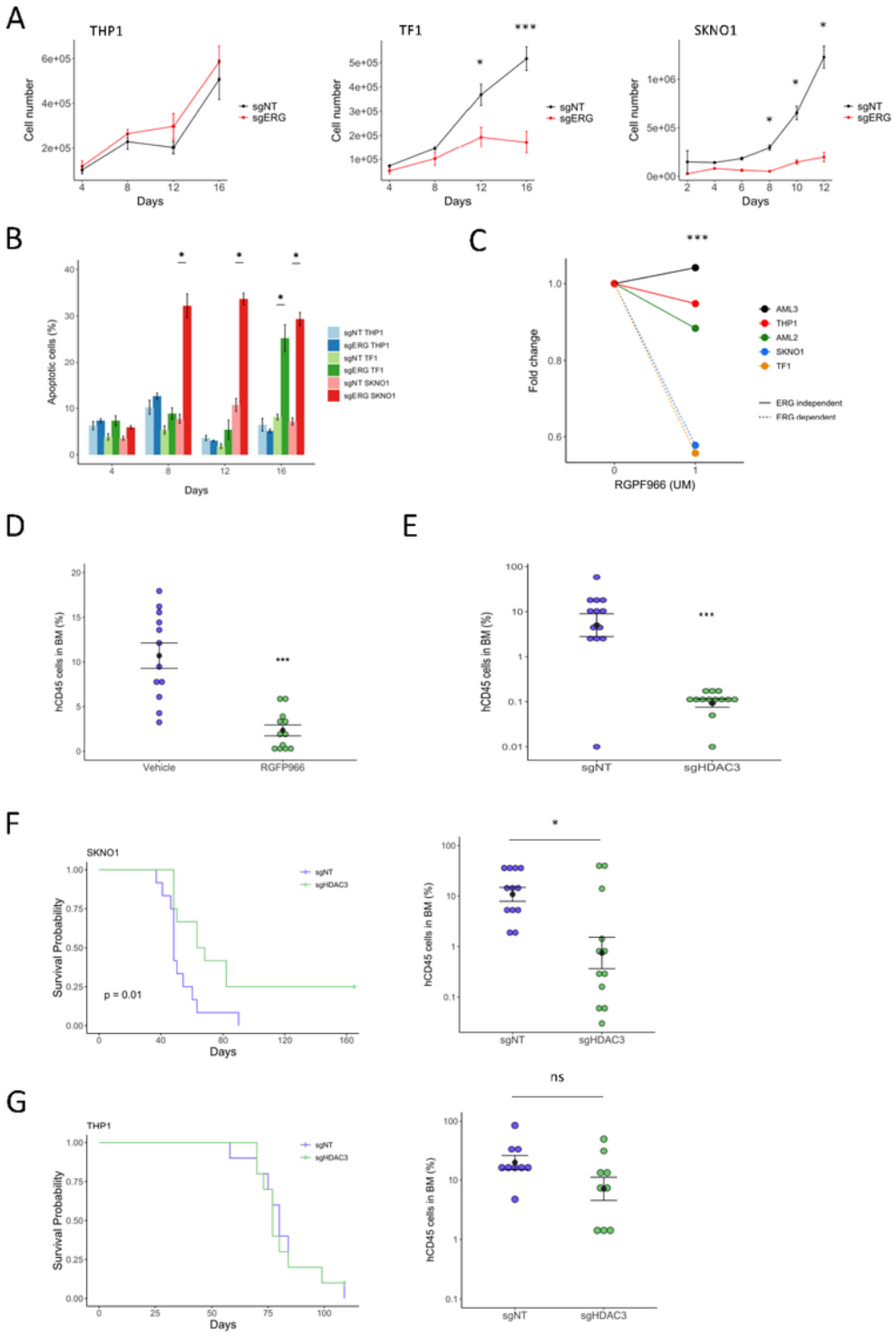

Figure 8

Figure 8

Pharmacologic and genetic HDAC3 inhibition results in reduced cell growth in high ERG expressing human AML cells *in vitro* and *in vivo*.

A. Cell growth curves following ERG knockout using CRISPR-Cas9 system.

B. Assessment of degree of apoptosis as a function of cell type and days in culture (n=3 in each group, Data are represented as mean ± SEM, Wilcoxson test).

C. HDAC3 inhibition using RGFP966 in low and high ERG expressing AML cell lines. Mean number of cells relative to RGFP966 concentration 0 after 48 hours in culture. T-tests, n=3 in each group.

D. The effect of HDAC3 inhibition on SKNO1 cells *in vivo*. NSG mice were transplanted with 250K SKNO1 cells and treated with 15mg/kg RGFP966 once daily intraperitoneally for 21 days from day 2 after transplant. (n=12 in each group, t-test, mean and standard error). The bone marrow percentage of human CD45 cells was used to assess disease burden.

E. Inhibition of HDAC3 using CRISPR-dCas9 system in SKNO1 cells. The bone marrow percentage of human CD45 cells was used to assess disease burden.

(n=12 in each group, Wilcoxon test, mean and standard error).

F. Survival curve of NSG mice transplanted with SKNO1 cells after CRISPR-dCas9 targeting of HDAC3 (left panel, n=12 in each group, log-rank test, P=0.01). The percentage of bone marrow hCD45 cells as a measure of disease burden (right panel, Wilcoxon test, p=0.012).

G. Survival curve of NSG mice transplanted with THP1 cells after CRISPR-dCas9 targeting of HDAC3 (left panel, n=10 in each group). The percentage of bone marrow hCD45 cells as a measure of disease burden (right panel, flow cytometry analysis for n=9 in each group, Wilcoxon test).

sgNT indicates non targeting guide. * $p<0.05$, ** $p<0.01$, *** $P<0.001$.

Supplementary Files

This is a list of supplementary files associated with this preprint. Click to download.

- supplemental.finalcopy.pdf